AIMS Mathematics, 11(11): 38609–38652.
DOI: 10.3934/math.20261490
Received: 25 June 2026
Revised: 16 August 2026
Accepted: 07 September 2026
Published: 19 November 2026

https://www.aimspress.com/journal/Math

Research article

Soliton interactions, bifurcations, and chaos in the (2+1)-dimensional KP-BBM equation for diffusive long waves in stratified media

Kalim U. Tariq[1,2,3,*], **R. Nadir Tufail**[2] **and Mohammed Ahmed Alomair**[4,*]

[1] Department of Mathematics, Faculty of Arts and Sciences, Yildiz Technical University, Davutpasa Campus, 34220, Esenler, Istanbul, Turkiye

[2] Department of Mathematics, Mirpur University of Science and Technology, Mirpur-10250 (AJK), Pakistan

[3] Research Center of Applied Mathematics, Khazar University, Baku, Azerbaijan

[4] Department of Quantitative Methods, School of Business, King Faisal University, Al-Ahsa 31982, Saudi Arabia

* **Correspondence:** Email: kalimulhaq@must.edu.pk; ma.alomair@kfu.edu.sa.

Abstract: In this study, the (2+1)-dimensional Kadomtsev-Petviashvili-Benjamin-Bona-Mahony (KP-BBM) equation representing diffusive long waves and bidirectional compact structures in dissipative stratified media is investigated analytically. The bilinear representation, which immediately produces lump solutions, periodic waves interacting with double strip solitons, and lump interactions with single or double strip solitons, is provided by Hirota's bilinear formalism. In addition, we use the Adomian decomposition methodology for numerical simulations, and the (G'/G^2)-expansion method provides additional accurate traveling-wave solutions. Phase-plane analysis and a traveling-wave reduction reveal the fundamental dynamics of the system. We use phase portraits, time series, Poincaré sections, and Lyapunov exponents to analyze bifurcations and the change from periodic to chaotic motion; further stability and sensitivity tests verify the robustness of the wave structures. The two- and three-dimensional visualizations of the solutions show that the model has a wide variety of soliton types, including bright, dark, rational, periodic, and elliptic functions. Overall, these results sharpen our understanding of the complex nonlinear behavior and propagation properties inherent in the KP-BBM equation.

Keywords: solitons; Hirota's bilinear method; bifurcation analysis; phase portraits; chaos detection; Lyapunov exponents; sensitivity and stability analysis; Adomian decomposition method
Mathematics Subject Classification: 35Rxx, 35Qxx, 35Q51

1. Introduction

Nonlinear partial differential equations (NPDEs) have grown in popularity over the last few decades due to their significant applications in engineering and physical sciences. In recent years, the study of integrable properties and the construction of soliton solutions for nonlinear evolution equations (NLEEs) have played an important role in a variety of physical and mathematical phenomena. The study of the physical nature and geometry of governing models may be more effectively accomplished in nonlinear wave dynamics through the use of processes including convection, dissipation, diffusion, and dispersion. NLEEs have many applications in nonlinear sciences such as optics [1], ocean engineering [2], turbulence theory, chaos theory [3], solitary waves theory [4], fluid dynamics [5], fluid mechanics [6], condensed matter physics [7], plasma physics [8], optical fibers [9], nonlinear optics [10], chemical physics, water waves [11], and many other fields.

NLEEs can be found in several fields of nonlinear sciences, including hydrodynamics, molecular biology, quantum mechanics, plasma physics, nonlinear optics, and applied mathematics. Many nonlinear physical and mathematical phenomena are known to depend critically on the discovery of soliton solutions for the NLEEs. To address these kinds of nonlinear models, a number of analytical and semi-analytical methods have been developed in recent years, including the the Bäcklund transformation [12], the variable separation technique [13], the Darboux transformation [14], the exp-function approach [15], the Hirota bilinear approach [16], the inverse scattering technique [17], the Adomian decomposition technique [18], the improved F-expansion approach [19], and the *tan* hyperbolic technique [20].

The (2+1)-dimensional Kadomtsev-Petviashvili-Benjamin-Bona-Mahony (KP-BBM) equation describes diffusive long waves and bidirectional compact structures that arise in stratified dissipative media. Hirota's bilinear approach has proven effective in constructing lump and multi-soliton solutions for this class of systems [21]. A combination of analytical and numerical treatments has also deepened our understanding of lump interactions and rogue wave phenomena [22]. Solution methods based on algebraic expansions, such as the (G'/G^2)-technique, produce a broad spectrum of traveling waves including bright, dark, rational, and elliptic profiles. In the recent past, phase portraits, Poincaré sections, and Lyapunov exponents have been used in bifurcation analysis and chaos diagnostics to detect transitions from periodic to chaotic regimes [23].

We focus here on constructing invariant soliton solutions to the (2+1)-dimensional KP-BBM model expressed as

$$\Omega_{xt} + \Omega_{xx} + \alpha(\Omega^2)_{xx} + \beta\Omega_{xxxt} + \gamma\Omega_{yy} = 0, \tag{1.1}$$

where α, β, and γ are real constants. This model accounts for dissipative effects in stratified media as well as bidirectional long-wave propagation and compact structures in nonlinear dispersive systems. Soliton pulses are steady and persistent when nonlinear convection and dispersion are in balance. Equation (1.1) draws from the Kadomtsev-Petviashvili (KP) equation [24]

$$(\Omega_t + 6\Omega\Omega_x + \Omega_{xxx})_x - \Omega_{yy} = 0, \tag{1.2}$$

and the BBM equation [25]

$$\Omega_t + \Omega_x + \Omega\Omega_x + \Omega_{xxt} = 0. \tag{1.3}$$

Moderate transverse fluctuations of unidirectional Korteweg-de Vries (KdV) solitons along the x-axis are captured by the KP equation [26], which is a prototype integrable system and is frequently thought of as the two-dimensional extension of the KdV model. It explains how long waves that need a transverse coordinate evolve gradually and nonlinearly. Weak dissipation and quadratic nonlinearity work together to model poorly diffusive waves under the paraxial wave approximation. Variational stability of energy minimizers, two-dimensional shallow-water dynamics [27], and ion-acoustic waves in dusty plasmas [28] are just a few of the many applications of the KP equation. It also governs quasi-one-dimensional shallow-water waves in ferromagnetic media when surface tension and viscous effects remain negligible. The BBM equation [29], on the other hand, provides a reliable approximation for unidirectional propagation of small-amplitude long waves in channels where transverse variation may be neglected. It is closely related to the KdV model for long surface waves with compact structure. The BBM equation has been thoroughly examined in contexts such as hydromagnetic waves, drift waves in cold plasmas, Rossby waves in rotating fluids, and acoustic-gravity waves in compressible media [30].

A brief overview of the relevant literature for the KP-BBM equation (1.1) is provided below. Wazwaz developed new compact and noncompact variants of the KP-BBM and the Zakharov-Kuznetsov BBM models using the extended tanh approach, which is an extension of the tanh series [31]. With respect to the conservation law, Saut and Tzvetkov obtained the localized solitary solitons using global well-posedness structures and generated specific soliton solutions based on the appropriate choice of arbitrary functions [32]. By suggesting the generalized (G'/G) expansion approach of the Riccati problem, Alam and Akbar constructed soliton-like solutions by symbolic computation [33]. Also, Tang et al. obtained the soliton solutions of the KP-BBM problem by using bifurcations of traveling wave solitons [34]. Using the Hirota bilinear technique and symbolic computing, certain lump solitons, lump-kink solitons, and breather-wave solitons were investigated in [35].

Moreover, in an outstanding study, Tan et al. [36] proposed the Landau-Lifshitz-Gilbert model to investigate the interaction and propagation of magnetic solitons in a ferromagnetic thin film, and Deng et al. [37] study analytical structures for determining the magnetic breathers and the rogue wave solitons. Similarly, Deng et al. [38] used the Hirota bilinear approach to investigate the collision process among lump and stripe solitons in the (2+1)-dimensional Caudrey-Dodd-Gibbon Kotera-Sawada model. The Boussinesq water wave model, which uses the Lie symmetry technique to predict the propagation of long waves in shallow water, was studied by Tian [39]. Tian and associates have investigated the KdV model to increase the shallow water wave amplitude in fluids [40]. Additionally, Tian and colleagues worked on a wide range of interesting topics, as evidenced by works such as the nonlinear Schrödinger model's scattering and inverse scattering problems [41], the Hirota model's rogue waves using Darboux transformation [42], the variable-coefficient BKP model using the Hirota bilinear technique [43], a cylindrical KP equation using a novel gauge transformation [44], and the creation of a Darboux transformation for the NLS model [45].

1.1. The significance and novelty of the present study

This study is significant as it unifies the treatment of dissipative stratified long-wave dynamics using the (2+1)-dimensional KP-BBM equation, connecting physically realistic layering and damping effects with conservative integrable models. Oceanic internal waves, atmospheric flows, and plasma systems are directly affected by this. Hirota's bilinear formalism, the (G'/G^2)-expansion, Adomian

decomposition, and phase-plane bifurcation analysis are all conceptually integrated into a cohesive framework. The originality of the current work is briefly described as follows: (i) It builds lump-double strip and periodic-double strip solutions for the first time in this dissipative setting; (ii) it reveals a distinct periodic-to-chaotic transition through bifurcation diagrams, Poincaré sections, and Lyapunov exponents, a dynamical feature that was previously missed; (iii) it reports an extraordinarily broad soliton taxonomy of bright, dark, rational, periodic, and elliptic-function profiles emerging from the same model; and (iv) it offers rigorous stability and sensitivity analysis that validate the physical resilience of these recently discovered multi-stripe and chaotic structures. Together, these findings promote practical wave prediction as well as nonlinear wave theory; for details see Figure 1.

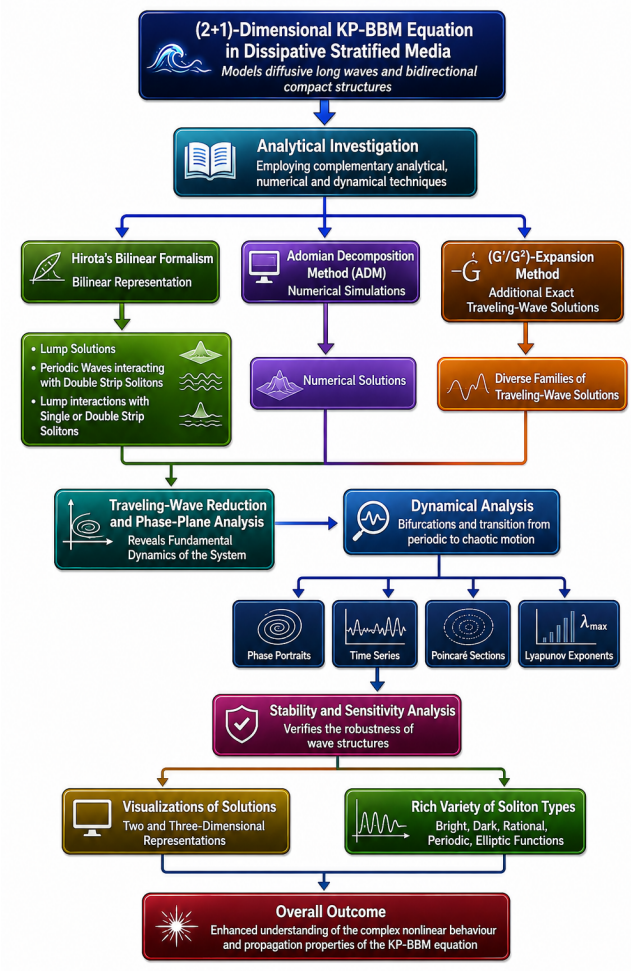


Figure 1. Schematic workflow for analyzing the (2 + 1)-dimensional KP-BBM equation.

The remainder of this paper is organized as follows: The bilinear form for the governing model is presented in Section 2, while the Hirota's bilinear approach is implemented in Section 3, and the $(\mathbb{G}'/\mathbb{G}^2)$-expansion method is utilized in Section 4. In Section 5, numerical results are presented. Stability and sensitivity studies are covered in Sections 6 and 7, respectively, while Section 8 presents the dynamical analysis. In Section 9, we provide physical interpretations of the solution profiles, and in the last section, we summarize our results.

2. Bilinear form for the governing model (1.1)

In 1971, Hirota [46] originally introduced the bilinear method for developing numerous solutions to nonlinear evolution models. The fundamental concept of this approach is to modify the NLEE so that the unknown function appears bilinearly by using a dependent variable transformation. The bilinear approach is a widely utilized and fundamental technique for solving NPDEs. The fundamental idea behind this method is to apply the proper structure to transform the governing model into bilinear form. The bilinear forms can then be used to establish the lump, breather, periodic, kink, N-soliton, rational, and other soliton solutions [47].

To obtain the bilinear form of (1.1), we employ the transformation

$$\Omega(x, y, t) = 2(\ln F)_{xx}, \tag{2.1}$$

where $F = F(x, y, t)$ is a real-valued function.

Substituting (2.1) into (1.1) and letting $q = \ln F$, we obtain

$$q_{xt} + q_{xx} + 2\alpha q_{xx}^2 + \beta q_{xxxt} + \gamma q_{yy} = 0, \tag{2.2}$$

where we have integrated twice with respect to x and set the integration functions to zero. This is consistent with solutions that decay as $|x| \to \infty$, for which the integration constants vanish.

We implement the standard Hirota identities [48] with the bilinear operator D defined as

$$D_x^\alpha D_t^\beta (u \cdot v) = \left(\frac{\partial}{\partial x} - \frac{\partial}{\partial x'}\right)^\alpha \left(\frac{\partial}{\partial t} - \frac{\partial}{\partial t'}\right)^\beta \times u(x, t) \cdot v(x', t')|_{x=x', t=t'}. \tag{2.3}$$

After simplification and multiplication by $2F^4$, Eq (2.2) becomes

$$\begin{aligned} &F^2(FF_{xt} - F_xF_t) + F^2(FF_{xx} - F_x^2) + \gamma F^2(FF_{yy} - F_y^2) \\ &+ \beta F^2(FF_{xxxt} - 3F_xF_{xxt} + 3F_{xx}F_{xt} - F_tF_{xxx}) \\ &+ \alpha(FF_{xx} - F_x^2)^2 - 3\beta(FF_{xx} - F_x^2)(FF_{xt} - F_xF_t) = 0. \end{aligned} \tag{2.4}$$

Using the Hirota operator notation, Eq (2.4) can be written compactly as

$$F^2\left(D_xD_t + D_x^2 + \beta D_x^3D_t + \gamma D_y^2\right)F \cdot F + \alpha(D_x^2F \cdot F)^2 - 3\beta(D_x^2F \cdot F)(D_xD_tF \cdot F) = 0. \tag{2.5}$$

Remark 2.1. Equation (2.5) is the correct representation for general values of the parameters α and β. It is important to note that this form is not purely bilinear due to the presence of the last two terms involving products of Hirota derivatives. The standard bilinear formulation is only recovered under specific conditions.

Remark 2.2. In the special case where the parameters satisfy the constraint

$$\alpha = 3\beta, \tag{2.6}$$

and we restrict our attention to traveling wave solutions of the form $q = q(\xi)$ with $\xi = x + ct + dy$, Eq (2.5) reduces to the standard bilinear form

$$\left(D_xD_t + D_x^2 + \beta D_x^3D_t + \gamma D_y^2\right)F \cdot F = 0. \tag{2.7}$$

Under these conditions, Eq (2.7) expands to

$$\begin{aligned} &FF_{xt} - F_xF_t + FF_{xx} - F_x^2 + \gamma(FF_{yy} - F_y^2) \\ &+ \beta(FF_{xxxt} - 3F_xF_{xxt} + 3F_{xx}F_{xt} - F_tF_{xxx}) = 0. \end{aligned} \tag{2.8}$$

In the subsequent sections, we will use the bilinear form (2.7) with the parameter constraint $\alpha = 3\beta$ to construct various soliton solutions of the KP-BBM equation (1.1). All solutions obtained will be verified by direct substitution into the original equation.

3. Applications of the Hirota bilinear technique

In this part, we use the bilinear form of the governing model provided in (2.7) to derive a number of intriguing solutions using the Hirota bilinear technique. It is important to emphasize that all solutions presented in this section are constructed under the parameter constraint $\alpha = 3\beta$ and for traveling wave or localized solutions, as discussed in the previous section. For these cases, the bilinear form (2.7) is valid and equivalent to the original governing equation (1.1).

3.1. Periodic wave solitons

Let us assume the function F is given by

$$F = \xi_0 + e^{-\eta_1}\xi_1 + e^{\eta_1}\xi_2 + \xi_3 \cos(\eta_2), \tag{3.1}$$

such that

$$\eta_1 = \alpha_0 + \alpha_1 x + \alpha_2 y + \alpha_3 t, \quad \eta_2 = \beta_0 + \beta_1 x + \beta_2 y + \beta_3 t,$$

where α_i and β_i are constants. Substituting (3.1) into (2.7), we have several equations. By solving these equations, we obtain the following results:

Case 1:

$$\alpha_3 = -\frac{\alpha_2^2\gamma + \alpha\alpha_1^2 + \alpha_1^2}{\alpha_1\left(\alpha_1^2\beta - 3\beta + 1\right)}, \ \xi_3 = 0.$$

With these values, (3.1) provides

$$\begin{aligned} F \ = \ & \xi_0 + \xi_1 \exp\left(-\alpha_0 + \frac{t\left(\alpha_2^2\gamma + \alpha\alpha_1^2 + \alpha_1^2\right)}{\alpha_1\left(\alpha_1^2\beta - 3\beta + 1\right)} - \alpha_1 x - \alpha_2 y\right) \\ & + \xi_2 \exp\left(\alpha_0 - \frac{t\left(\alpha_2^2\gamma + \alpha\alpha_1^2 + \alpha_1^2\right)}{\alpha_1\left(\alpha_1^2\beta - 3\beta + 1\right)} + \alpha_1 x + \alpha_2 y\right). \end{aligned} \tag{3.2}$$

Substituting (3.2) into (2.1) gives the solution $\Omega_1(x, y, t)$.

Case 2:

$$\alpha_2 = \frac{i\sqrt{\alpha_1}\sqrt{\alpha_3\alpha_1^2\beta - 3\alpha_3\beta + \alpha\alpha_1 + \alpha_1 + \alpha_3}}{\sqrt{\gamma}}, \ \xi_3 = 0.$$

With these values, (3.1) provides

$$F = \xi_0 + \xi_1 \exp\left(-\alpha_0 - \alpha_3 t - \alpha_1 x - \frac{i\sqrt{\alpha_1} y \sqrt{\alpha_3 \alpha_1^2 \beta - 3\alpha_3 \beta + \alpha\alpha_1 + \alpha_1 + \alpha_3}}{\sqrt{\gamma}}\right)$$
$$+\xi_2 \exp\left(\alpha_0 + \alpha_3 t + \alpha_1 x + \frac{i\sqrt{\alpha_1} y \sqrt{\alpha_3 \alpha_1^2 \beta - 3\alpha_3 \beta + \alpha\alpha_1 + \alpha_1 + \alpha_3}}{\sqrt{\gamma}}\right). \tag{3.3}$$

Substituting (3.3) into (2.1) gives the solution $\Omega_2(x, y, t)$.

3.2. Interactions of a lump wave with a strip soliton

Let us take the function F to be

$$F = \xi_0 + \xi_1 \eta_1^2 + \xi_2 \eta_2^2 + \xi_3 e^{\eta_3}, \tag{3.4}$$

such that

$$\eta_1 = \alpha_0 + \alpha_1 x + \alpha_2 y + \alpha_3 t, \quad \eta_2 = \beta_0 + \beta_1 x + \beta_2 y + \beta_3 t, \quad \eta_3 = \gamma_0 + \gamma_1 x + \gamma_2 y + \gamma_3 t,$$

where α_i, β_i, and γ_i are constants. Substituting (3.4) into (2.7), we have several equations. By solving these equations, we obtain the following results:

Case 1:

$$\gamma_3 = -\frac{\alpha\gamma_1^2 + \gamma_1^2 + \gamma\gamma_2^2}{\gamma_1\left(\beta\gamma_1^2 - 3\beta + 1\right)}, \ \xi_1 = 0, \ \xi_2 = 0.$$

With these values, (3.4) provides

$$F = \xi_0 + \xi_3 \exp\left(\gamma_0 - \frac{t\left(\alpha\gamma_1^2 + \gamma_1^2 + \gamma\gamma_2^2\right)}{\gamma_1\left(\beta\gamma_1^2 - 3\beta + 1\right)} + \gamma_1 x + \gamma_2 y\right). \tag{3.5}$$

Substituting (3.5) into (2.1), we have

$$\Omega_3(x, y, t) = \frac{2\gamma_1^2\xi_3 \exp\left(\gamma_0 - \frac{t\left(\alpha\gamma_1^2+\gamma_1^2+\gamma\gamma_2^2\right)}{\gamma_1\left(\beta\gamma_1^2-3\beta+1\right)} + \gamma_1 x + \gamma_2 y\right)}{\xi_3 \exp\left(\gamma_0 - \frac{t\left(\alpha\gamma_1^2+\gamma_1^2+\gamma\gamma_2^2\right)}{\gamma_1\left(\beta\gamma_1^2-3\beta+1\right)} + \gamma_1 x + \gamma_2 y\right) + \xi_0}$$
$$-\frac{2\gamma_1^2\xi_3^2 \exp\left(2\gamma_0 - \frac{2t\left(\alpha\gamma_1^2+\gamma_1^2+\gamma\gamma_2^2\right)}{\gamma_1\left(\beta\gamma_1^2-3\beta+1\right)} + 2\gamma_1 x + 2\gamma_2 y\right)}{\left(\xi_3 \exp\left(\gamma_0 - \frac{t\left(\alpha\gamma_1^2+\gamma_1^2+\gamma\gamma_2^2\right)}{\gamma_1\left(\beta\gamma_1^2-3\beta+1\right)} + \gamma_1 x + \gamma_2 y\right) + \xi_0\right)^2}. \tag{3.6}$$

Case 2:

$$\alpha_3 = \frac{\alpha_1\left(\xi_2\left((\alpha+1)\beta_1^2 - \beta_2^2\gamma\right) + \alpha_2^2\gamma\xi_1\right) + 2\alpha_2\beta_1\beta_2\gamma\xi_2 + (\alpha+1)\alpha_1^3\xi_1}{(3\beta-1)\left(\alpha_1^2\xi_1 + \beta_1^2\xi_2\right)},$$

$$\beta_3 = \frac{2\alpha_2\alpha_1\beta_2\gamma\xi_1 + \beta_1\left(\xi_2\left((\alpha+1)\beta_1^2 + \beta_2^2\gamma\right) - \alpha_2^2\gamma\xi_1\right) + (\alpha+1)\alpha_1^2\beta_1\xi_1}{(3\beta-1)\left(\alpha_1^2\xi_1 + \beta_1^2\xi_2\right)},$$

$$\xi_0 = \frac{3\beta\left(\alpha_1^2\xi_1 + \beta_1^2\xi_2\right)}{\left(3\beta-1\right)\gamma\xi_1\xi_2\left(\alpha_2\beta_1 - \alpha_1\beta_2\right)^2}(\alpha\alpha_1^4\xi_1^2 + \alpha_1^4\xi_1^2 + 2\alpha\alpha_1^2\beta_1^2\xi_1\xi_2 + \alpha_2^2\alpha_1^2\gamma\xi_1^2 + 2\alpha_1^2\beta_1^2\xi_1\xi_2$$
$$-\alpha_2^2\beta_1^2\gamma\xi_1\xi_2 + 4\alpha_1\alpha_2\beta_2\beta_1\gamma\xi_1\xi_2 - \alpha_1^2\beta_2^2\gamma\xi_1\xi_2 + \alpha\beta_1^4\xi_2^2 + \beta_2^2\beta_1^2\gamma\xi_2^2 + \beta_1^4\xi_2^2),$$

$$\xi_3 = 0.$$

Substituting these values into (3.4) and (2.1) gives the solution $\Omega_4(x, y, t)$.

Case 3:

$$\alpha_3 = \frac{2\alpha_2^2\beta_1\gamma + 2\alpha\alpha_1^2\beta_1 + 2\alpha_1^2\beta_1 - 3\alpha_1^2\beta\beta_3 + \alpha_1^2\beta_3}{\alpha_1(3\beta-1)\beta_1},$$

$$\beta_2 = \frac{\alpha_2\beta_1}{\alpha_1},\ \xi_0 = 0,\ \xi_2 = -\frac{\alpha_1^2\xi_1}{\beta_1^2},\ \xi_3 = 0.$$

With these values, (3.4) provides

$$F = \xi_1\left(\alpha_0 + \frac{t\left(2\alpha_2^2\beta_1\gamma + 2\alpha\alpha_1^2\beta_1 + 2\alpha_1^2\beta_1 - 3\alpha_1^2\beta\beta_3 + \alpha_1^2\beta_3\right)}{\alpha_1(3\beta-1)\beta_1} + \alpha_1 x + \alpha_2 y\right)^2$$
$$-\frac{\alpha_1^2\xi_1\left(\beta_0 + \beta_3 t + \beta_1 x + \frac{\alpha_2\beta_1 y}{\alpha_1}\right)^2}{\beta_1^2}. \tag{3.7}$$

Substituting (3.7) into (2.1) gives the solution $\Omega_5(x, y, t)$.

Case 4:

$$\alpha_3 = \frac{\alpha_1\left(2\alpha\beta_1^2 + 2\beta_2^2\gamma + 2\beta_1^2 - 3\beta\beta_3\beta_1 + \beta_3\beta_1\right)}{(3\beta-1)\beta_1^2},$$

$$\alpha_2 = \frac{\alpha_1\beta_2}{\beta_1},\ \xi_0 = 0,\ \xi_2 = -\frac{\alpha_1^2\xi_1}{\beta_1^2},\ \xi_3 = 0.$$

With these values, (3.4) provides

$$F = \xi_1\left(\alpha_0 + \frac{\alpha_1 t\left(2\alpha\beta_1^2 + 2\beta_2^2\gamma + 2\beta_1^2 - 3\beta\beta_3\beta_1 + \beta_3\beta_1\right)}{(3\beta-1)\beta_1^2} + \alpha_1 x + \frac{\alpha_1\beta_2 y}{\beta_1}\right)^2$$
$$-\frac{\alpha_1^2\xi_1\left(\beta_0 + \beta_3 t + \beta_1 x + \beta_2 y\right)^2}{\beta_1^2}. \tag{3.8}$$

Substituting (3.8) into (2.1) gives the solution $\Omega_6(x, y, t)$.

3.3. Interaction of a lump wave with a double stripe soliton

Let us assume the function F is given by

$$F = \xi_0 + \xi_1\eta_1^2 + \xi_2\eta_2^2 + \xi_3\cosh(\eta_3). \tag{3.9}$$

Inserting (3.9) in (2.7), we have several equations. By solving these equations, we obtain the following results:

Case 1:

$$\gamma_3 = -\frac{\alpha\gamma_1^2 + \gamma_1^2 + \gamma\gamma_2^2}{\gamma_1\left(4\beta\gamma_1^2 - 3\beta + 1\right)},\ \xi_0 = 0,\ \xi_1 = 0,\ \xi_2 = 0.$$

With these values, (3.9) provides

$$F = \xi_3\cosh\left(\gamma_0 - \frac{t\left(\alpha\gamma_1^2 + \gamma_1^2 + \gamma\gamma_2^2\right)}{\gamma_1\left(4\beta\gamma_1^2 - 3\beta + 1\right)} + \gamma_1 x + \gamma_2 y\right). \tag{3.10}$$

Substituting (3.10) into (2.1), we have

$$\Omega_7(x,y,t) = 2\gamma_1^2\mathrm{sech}^2\left(\gamma_0 - \frac{t\left(\alpha\gamma_1^2 + \gamma_1^2 + \gamma\gamma_2^2\right)}{\gamma_1\left(4\beta\gamma_1^2 - 3\beta + 1\right)} + \gamma_1 x + \gamma_2 y\right). \tag{3.11}$$

Case 2:

$$\alpha_3 = \frac{-\alpha^2\alpha_1^4 + \alpha_2^4\gamma^2 - 2\alpha\alpha_1^4 - \alpha_1^4}{2\alpha_1\alpha_2^2(3\beta-1)\gamma},\ \beta_2 = -\frac{(\alpha+1)\alpha_1\beta_1}{\alpha_2\gamma},$$
$$\beta_3 = -\frac{\beta_1\left(-\alpha^2\alpha_1^4 + \alpha_2^4\gamma^2 - 2\alpha\alpha_1^4 - \alpha_1^4\right)}{2\alpha_1^2\alpha_2^2(3\beta-1)\gamma},\ \xi_2 = \frac{\alpha_1^2\xi_1}{\beta_1^2}.$$

With these values, (3.9) provides

$$\begin{aligned} F &= \xi_1\left(\alpha_0 + \frac{t\left(-\alpha^2\alpha_1^4 + \alpha_2^4\gamma^2 - 2\alpha\alpha_1^4 - \alpha_1^4\right)}{2\alpha_1\alpha_2^2(3\beta-1)\gamma} + \alpha_1 x + \alpha_2 y\right)^2 \\ &+ \frac{\alpha_1^2\xi_1\left(\beta_0 - \frac{\beta_1 t\left(-\alpha^2\alpha_1^4 + \alpha_2^4\gamma^2 - 2\alpha\alpha_1^4 - \alpha_1^4\right)}{2\alpha_1^2\alpha_2^2(3\beta-1)\gamma} + \beta_1 x - \frac{(\alpha+1)\alpha_1\beta_1 y}{\alpha_2\gamma}\right)^2}{\beta_1^2}. \end{aligned} \tag{3.12}$$

Substituting(3.12) into (2.1) gives the solution $\Omega_8(x,y,t)$.

Case 3:

$$\alpha_3 = \frac{2\alpha_2^2\beta_1\gamma + 2\alpha\alpha_1^2\beta_1 + 2\alpha_1^2\beta_1 - 3\alpha_1^2\beta\beta_3 + \alpha_1^2\beta_3}{\alpha_1(3\beta-1)\beta_1},$$
$$\beta_2 = \frac{\alpha_2\beta_1}{\alpha_1},\ \xi_0 = 0,\ \xi_2 = -\frac{\alpha_1^2\xi_1}{\beta_1^2},\ \xi_3 = 0.$$

With these values, (3.9) provides

$$F = \xi_1\left(\alpha_0 + \frac{t\left(2\alpha_2^2\beta_1\gamma + 2\alpha\alpha_1^2\beta_1 + 2\alpha_1^2\beta_1 - 3\alpha_1^2\beta\beta_3 + \alpha_1^2\beta_3\right)}{\alpha_1(3\beta-1)\beta_1} + \alpha_1 x + \alpha_2 y\right)^2 - \frac{\alpha_1^2\xi_1\left(\beta_0 + \beta_3 t + \beta_1 x + \frac{\alpha_2\beta_1 y}{\alpha_1}\right)^2}{\beta_1^2}. \tag{3.13}$$

Substituting (3.13) into (2.1) gives the solution $\Omega_9(x, y, t)$.

Case 4:

$$\gamma_2 = \frac{i\sqrt{\gamma_1}\sqrt{\alpha\gamma_1 + 4\beta\gamma_3\gamma_1^2 - 3\beta\gamma_3 + \gamma_1 + \gamma_3}}{\sqrt{\gamma}},\ \xi_0 = 0,\ \xi_1 = 0,\ \xi_2 = 0.$$

With these values, (3.9) provides

$$F = \xi_3\cosh\left(\gamma_0 + \gamma_3 t + \gamma_1 x + \frac{i\sqrt{\gamma_1}y\sqrt{\alpha\gamma_1 + 4\beta\gamma_3\gamma_1^2 - 3\beta\gamma_3 + \gamma_1 + \gamma_3}}{\sqrt{\gamma}}\right). \tag{3.14}$$

Substituting (3.14) into (2.1), we have

$$\Omega_{10}(x, y, t) = 2\gamma_1^2\mathrm{sech}^2\left(\gamma_0 + \gamma_3 t + \gamma_1 x + \frac{i\sqrt{\gamma_1}y\sqrt{\alpha\gamma_1 + 4\beta\gamma_3\gamma_1^2 - 3\beta\gamma_3 + \gamma_1 + \gamma_3}}{\sqrt{\gamma}}\right).$$

3.4. Interaction of a lump with periodic waves

Let us take the function F to be

$$F = \xi_0 + \xi_1\eta_1^2 + \xi_2\eta_2^2 + \xi_3\cos(\eta_3). \tag{3.15}$$

Inserting (3.15) in (2.7), we have several equations. By solving these equations, we obtain the following results:

Case 1:

$$\gamma_3 = -\frac{-\alpha\gamma_1^2 - \gamma_1^2 - \gamma\gamma_2^2}{\gamma_1\left(4\beta\gamma_1^2 + 3\beta - 1\right)},\ \ \xi_0 = 0,\ \ \xi_1 = 0,\ \ \xi_2 = 0.$$

With these values, (3.15) provides

$$F = \xi_3\cos\left(\gamma_0 - \frac{t\left(-\alpha\gamma_1^2 - \gamma_1^2 - \gamma\gamma_2^2\right)}{\gamma_1\left(4\beta\gamma_1^2 + 3\beta - 1\right)} + \gamma_1 x + \gamma_2 y\right). \tag{3.16}$$

Substituting (3.16) into (2.1), we have

$$\Omega_{11}(x, y, t) = -2\gamma_1^2\sec^2\left(\gamma_0 - \frac{t\left(-\alpha\gamma_1^2 - \gamma_1^2 - \gamma\gamma_2^2\right)}{\gamma_1\left(4\beta\gamma_1^2 + 3\beta - 1\right)} + \gamma_1 x + \gamma_2 y\right). \tag{3.17}$$

Case 2:

$$\alpha_3 = \frac{2\alpha_2^2\beta_1\gamma + 2\alpha\alpha_1^2\beta_1 + 2\alpha_1^2\beta_1 - 3\alpha_1^2\beta\beta_3 + \alpha_1^2\beta_3}{\alpha_1(3\beta-1)\beta_1},\ \xi_0 = 0,$$
$$\beta_2 = \frac{\alpha_2\beta_1}{\alpha_1},\ \xi_2 = -\frac{\alpha_1^2\xi_1}{\beta_1^2},\ \xi_3 = 0.$$

With these values, (3.15) provides

$$\begin{aligned} F &= \xi_1\left(\alpha_0 + \frac{t\left(2\alpha_2^2\beta_1\gamma + 2\alpha\alpha_1^2\beta_1 + 2\alpha_1^2\beta_1 - 3\alpha_1^2\beta\beta_3 + \alpha_1^2\beta_3\right)}{\alpha_1(3\beta-1)\beta_1} + \alpha_1 x + \alpha_2 y\right)^2 \\ &\quad - \frac{\alpha_1^2\xi_1\left(\beta_0 + \beta_3 t + \beta_1 x + \frac{\alpha_2\beta_1 y}{\alpha_1}\right)^2}{\beta_1^2}. \end{aligned} \tag{3.18}$$

Substituting (3.18) into (2.1) gives the solution $\Omega_{12}(x, y, t)$.

Case 3:

$$\gamma_2 = \frac{\sqrt{\gamma_1}\sqrt{-\alpha\gamma_1 + 4\beta\gamma_3\gamma_1^2 + 3\beta\gamma_3 - \gamma_1 - \gamma_3}}{\sqrt{\gamma}},\ \xi_0 = 0,\ \xi_1 = 0,\ \xi_2 = 0.$$

With these values, (3.15) provides

$$F = \xi_3 \cos\left(\gamma_0 + \gamma_3 t + \gamma_1 x + \frac{\sqrt{\gamma_1} y\sqrt{-\alpha\gamma_1 + 4\beta\gamma_3\gamma_1^2 + 3\beta\gamma_3 - \gamma_1 - \gamma_3}}{\sqrt{\gamma}}\right). \tag{3.19}$$

Substituting (3.19) into (2.1), we have

$$\Omega_{13}(x, y, t) = -2\gamma_1^2 \sec^2\left(\gamma_0 + \gamma_3 t + \gamma_1 x + \frac{\sqrt{\gamma_1} y\sqrt{-\alpha\gamma_1 + 4\beta\gamma_3\gamma_1^2 + 3\beta\gamma_3 - \gamma_1 - \gamma_3}}{\sqrt{\gamma}}\right).$$

Case 4:

$$\alpha_3 = \frac{-\alpha^2\alpha_1^4 + \alpha_2^4\gamma^2 - 2\alpha\alpha_1^4 - \alpha_1^4}{2\alpha_1\alpha_2^2(3\beta-1)\gamma},\ \beta_2 = -\frac{(\alpha+1)\alpha_1\beta_1}{\alpha_2\gamma}, \xi_0 = 0,$$
$$\beta_3 = -\frac{\beta_1\left(-\alpha^2\alpha_1^4 + \alpha_2^4\gamma^2 - 2\alpha\alpha_1^4 - \alpha_1^4\right)}{2\alpha_1^2\alpha_2^2(3\beta-1)\gamma},\ \xi_2 = \frac{\alpha_1^2\xi_1}{\beta_1^2},\ \xi_3 = 0.$$

With these values, (3.15) provides

$$\begin{aligned} F &= \xi_1\left(\alpha_0 + \frac{t\left(-\alpha^2\alpha_1^4 + \alpha_2^4\gamma^2 - 2\alpha\alpha_1^4 - \alpha_1^4\right)}{2\alpha_1\alpha_2^2(3\beta-1)\gamma} + \alpha_1 x + \alpha_2 y\right)^2 \\ &\quad + \frac{\alpha_1^2\xi_1\left(\beta_0 - \frac{\beta_1 t\left(-\alpha^2\alpha_1^4 + \alpha_2^4\gamma^2 - 2\alpha\alpha_1^4 - \alpha_1^4\right)}{2\alpha_1^2\alpha_2^2(3\beta-1)\gamma} + \beta_1 x - \frac{(\alpha+1)\alpha_1\beta_1 y}{\alpha_2\gamma}\right)^2}{\beta_1^2}. \end{aligned} \tag{3.20}$$

Substituting (3.20) into (2.1) gives the solution $\Omega_{14}(x, y, t)$.

3.5. Interaction of lump and periodic waves with a double stripe soliton

Let us assume the function F is given by

$$F = \xi_0 + \xi_1\eta_1^2 + \xi_2\cosh(\eta_2) + \xi_3\cos(\eta_3). \tag{3.21}$$

Inserting (3.21) in (2.7), we have several equations. By solving these equations, we obtain the following results:

Case 1:

$$\beta_1 = i\gamma_1,\ \beta_3 = \frac{i\left(\alpha\gamma_1^2+\gamma_1^2+\gamma\gamma_2^2\right)}{\gamma_1\left(4\beta\gamma_1^2+3\beta-1\right)},\ \gamma_3 = \frac{\alpha\gamma_1^2+\gamma_1^2+\gamma\gamma_2^2}{\gamma_1\left(4\beta\gamma_1^2+3\beta-1\right)},\ \xi_0 = 0,\ \xi_1 = 0,$$

$$\begin{aligned}\beta_2 = -\frac{1}{2\gamma\gamma_2}(&i\gamma_1^2 + i\alpha\gamma_1^2 - \frac{i\alpha\gamma_1^2}{-4\beta\gamma_1^2-3\beta+1} - \frac{i\gamma_1^2}{-4\beta\gamma_1^2-3\beta+1} + \frac{4i\alpha\beta\gamma_1^4}{-4\beta\gamma_1^2-3\beta+1}\\ &+\frac{3i\alpha\beta\gamma_1^2}{-4\beta\gamma_1^2-3\beta+1} + \frac{4i\beta\gamma_1^4}{-4\beta\gamma_1^2-3\beta+1} + \frac{3i\beta\gamma_1^2}{-4\beta\gamma_1^2-3\beta+1} + \frac{4i\beta\gamma\gamma_1^2\gamma_2^2}{-4\beta\gamma_1^2-3\beta+1}\\ &-\frac{i\gamma\gamma_2^2}{-4\beta\gamma_1^2-3\beta+1} + \frac{3i\beta\gamma\gamma_2^2}{-4\beta\gamma_1^2-3\beta+1} - i\gamma\gamma_2^2).\end{aligned}$$

Substituting these values into (3.21) and (2.1) gives the solution $\Omega_{15}(x, y, t)$.

Case 2:

$$\beta_3 = \frac{-\alpha\beta_1^2-\beta_2^2\gamma-\beta_1^2}{\beta_1\left(4\beta\beta_1^2-3\beta+1\right)},\ \gamma_1 = i\beta_1,\ \gamma_3 = -\frac{i\left(\alpha\beta_1^2+\beta_2^2\gamma+\beta_1^2\right)}{\beta_1\left(4\beta\beta_1^2-3\beta+1\right)},\ \xi_0 = 0,\ \xi_1 = 0,$$

$$\begin{aligned}\gamma_2 = \frac{1}{2\beta_2\gamma}(&-i\alpha\beta_1^2 - i\beta_1^2 + \frac{i\alpha\beta_1^2}{4\beta\beta_1^2-3\beta+1} + \frac{i\beta_1^2}{4\beta\beta_1^2-3\beta+1} + \frac{4i\alpha\beta\beta_1^4}{4\beta\beta_1^2-3\beta+1}\\ &-\frac{3i\alpha\beta\beta_1^2}{4\beta\beta_1^2-3\beta+1} + \frac{4i\beta\beta_1^4}{4\beta\beta_1^2-3\beta+1} - \frac{3i\beta\beta_1^2}{4\beta\beta_1^2-3\beta+1} + i\beta_2^2\gamma\\ &+\frac{4i\beta\beta_1^2\beta_2^2\gamma}{4\beta\beta_1^2-3\beta+1} + \frac{i\beta_2^2\gamma}{4\beta\beta_1^2-3\beta+1} - \frac{3i\beta\beta_2^2\gamma}{4\beta\beta_1^2-3\beta+1}).\end{aligned}$$

Substituting these values into (3.21) and (2.1) gives the solution $\Omega_{16}(x, y, t)$.

Remark: All solutions presented above have been verified by direct substitution into the original governing equation (1.1) under the condition $\alpha = 3\beta$. The parameter α in the solutions should be understood as 3β for consistency with the bilinear form derivation. The solutions provide a rich variety of wave phenomena including periodic waves, lump waves, stripe solitons, and their various interactions.

3.6. Soliton dynamics

Figures 2 and 3 collect different soliton behaviors in the (2+1)-dimensional KP-BBM equation (1.1). Together they show how wave energy can organize into repeating patterns, narrow strips, interacting peaks, or isolated humps.

Figure 2 focuses on periodic and strip-like solitons. Figure 2(a) gives a two-dimensional contour view of a periodic soliton: The wave peaks repeat at regular intervals, much like a grid of hills and valleys. Figure 2(b) shows the same case in three dimensions, where the oscillations rise and fall smoothly without abrupt changes. Another 2D periodic contour is shown in Figure 2(e); however, this one has a slightly different wave alignment than the previous one, indicating a different phase. Figure 2(f) shifts to a more complex three-dimensional periodic soliton; multiple peaks interact with each other, and their heights differ significantly across the plot. In 2D, Figure 2(c) shows a strip-like soliton with long, narrow wavefronts that resemble stretched ridges. The 3D image of that strip soliton, where energy remains tightly focused along an elevated, straight line, is shown in Figure 2(d).

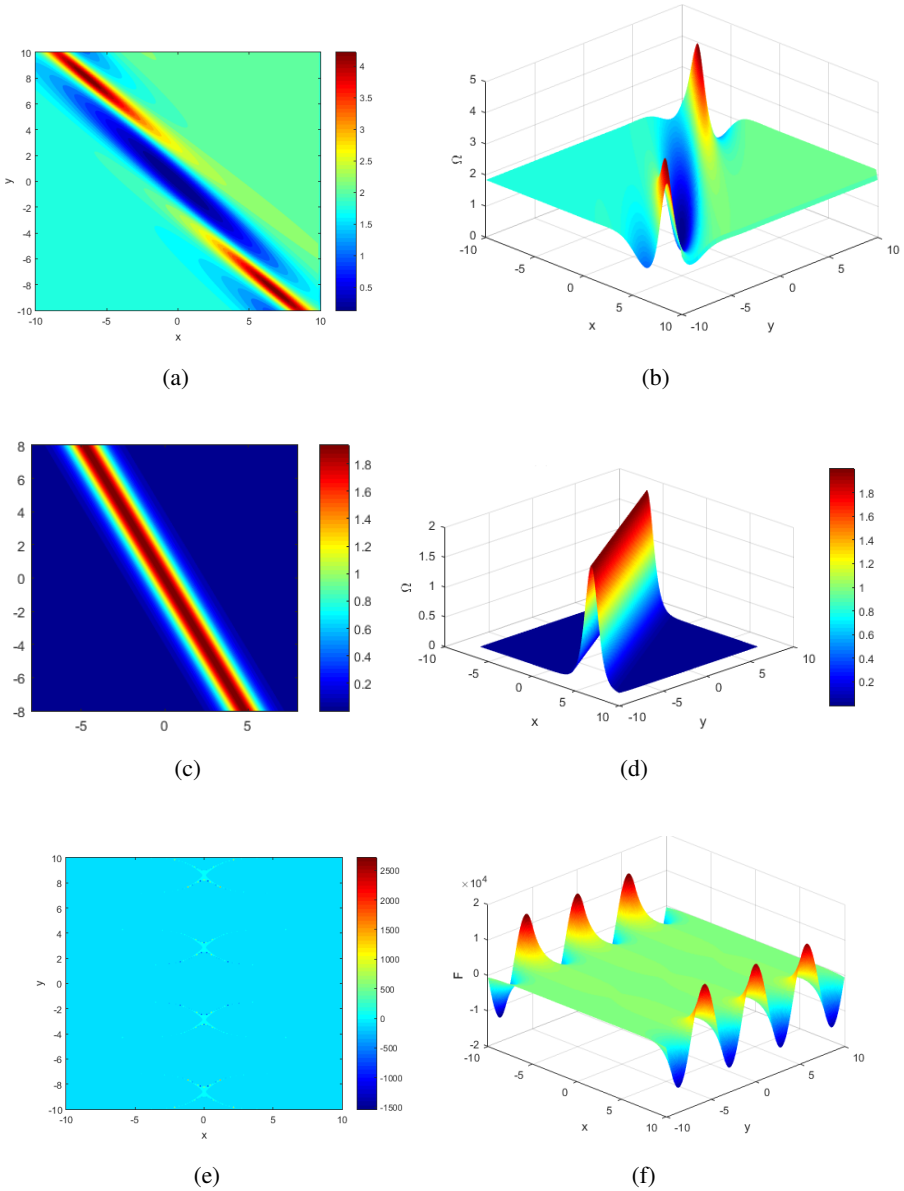


Figure 2. Visualization of periodic soliton $\Omega_2(x, y, t)$, strip-like soliton $\Omega_4(x, y, t)$, and interaction of a lump wave with double-stripe soliton $\Omega_8(x, y, t)$.

Strip, mixed-interaction, and lump solitons are shown in Figure 3. Figure 3(a) shows a 2D contour of a strip soliton once more; the wave front is still thin and stretched out, but the direction or width is different from that in previous examples. This strip soliton is depicted in three dimensions in Figure 3(b), where energy is tightly retained along a steep ridge. A mixed soliton interaction in 2D is introduced by Figure 3(c), where two or more wave patterns overlap, intersect, and interfere to provide a more convoluted contour than in the pure periodic or strip situations. The three-dimensional representation of that mixed interaction is shown in Figure 3(d), which shows how the solitons combine and then split apart as one travels around the surface. In contrast to the extended stripes or recurring waves, the lump soliton in Figure 3(e) remains contained within a single rounded hump in two dimensions. The 3D image of the lump soliton is seen in Figure 3(f), where a tall, isolated peak rises above the background and gradually fades away in all directions.

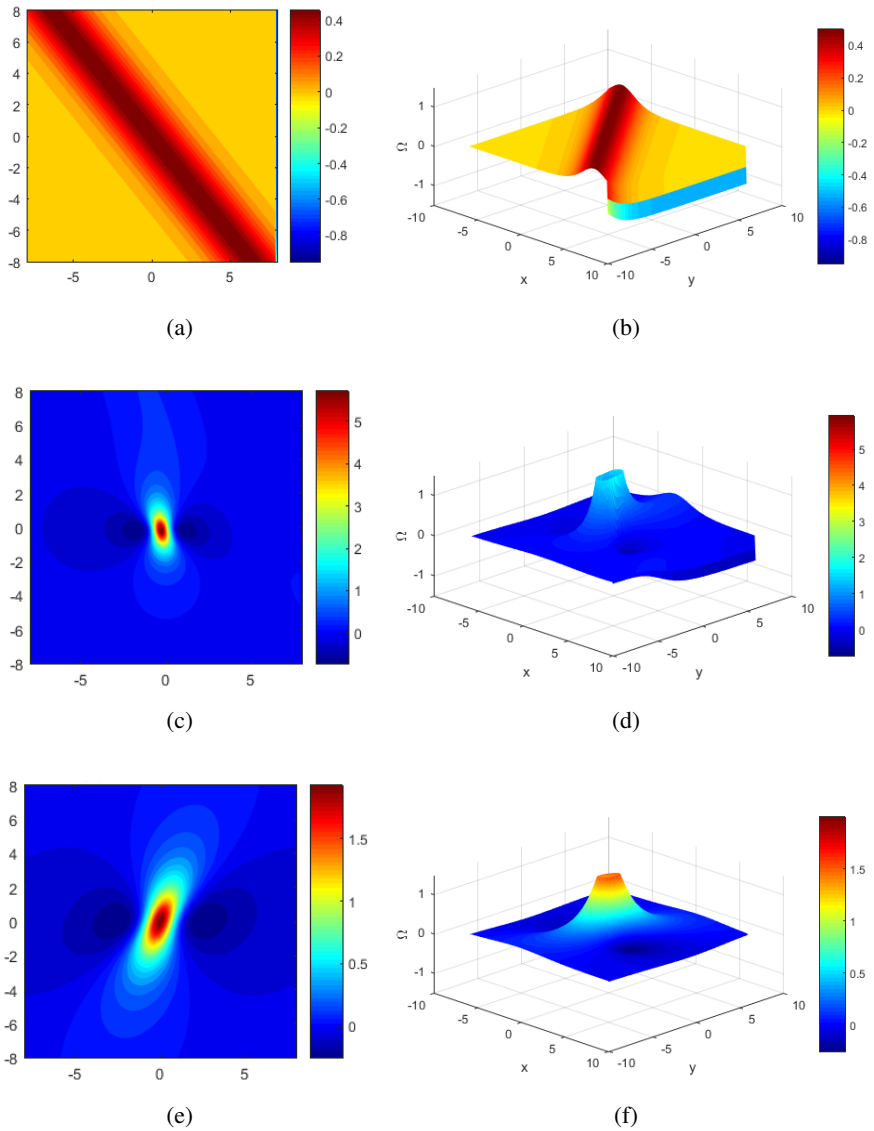


Figure 3. Visualization of strip soliton $\Omega_{12}(x, y, t)$, interaction of a lump with periodic waves $\Omega_{14}(x, y, t)$, and interaction of lump and periodic wave with a double-stripe soliton $\Omega_{15}(x, y, t)$.

4. Traveling wave solitons

In this section, the $(\mathbb{G}'/\mathbb{G}^2)$-expansion method will be used to establish the traveling wave solitons for the governing model (1.1). Hence, we use the transformation given by

$$\Omega(x, y, t) = V(\psi), \qquad \psi = ax + by - \lambda t, \tag{4.1}$$

where a and b are parameters, and λ is the wave velocity. Applying the transformation (4.1) to (1.1), we obtain

$$-a^3\beta\lambda V^{(4)}(\psi) + V''(\psi)\left(a^2 - a\lambda + b^2\gamma\right) + 2\alpha a^2\left(V(\psi)V''(\psi) + V'(\psi)^2\right) = 0.$$

Integrating it twice, we attain

$$-a^3\beta\lambda V''(\psi) + V(\psi)\left(a^2 - a\lambda + b^2\gamma\right) + \alpha a^2 V(\psi)^2 = 0. \tag{4.2}$$

We assume the following solution to (4.2) using the considered method:

$$V(\psi) = \sum_{i=0}^{n} \rho_i \left(\frac{\mathbb{G}'(\psi)}{\mathbb{G}(\psi)^2}\right)^i + \sum_{j=1}^{n} \varrho_j \left(\frac{\mathbb{G}'(\psi)}{\mathbb{G}(\psi)^2}\right)^{-j}, \tag{4.3}$$

such that ρ_i and ϱ_j are constants, while $\frac{G'(\psi)}{G(\psi)^2}$ satisfies

$$\left(\frac{\mathbb{G}'(\psi)}{\mathbb{G}(\psi)^2}\right)' = \omega + \kappa\left(\frac{\mathbb{G}'(\psi)}{\mathbb{G}(\psi)^2}\right)^2, \tag{4.4}$$

while ω and κ are parameters. As a result, we demonstrate the following results:

Result I. Considering $\omega\kappa > 0$, we obtain

$$\frac{G'(\psi)}{G(\psi)^2} = \sqrt{\frac{\omega}{\kappa}}\frac{\chi_2 \sin\left(\psi\sqrt{\kappa\omega}\right) + \chi_1 \cos\left(\psi\sqrt{\kappa\omega}\right)}{\chi_2 \cos\left(\psi\sqrt{\kappa\omega}\right) - \chi_1 \sin\left(\psi\sqrt{\kappa\omega}\right)}.$$

Result II. Considering $\omega\kappa < 0$, we obtain

$$\frac{\mathbb{G}'(\psi)}{\mathbb{G}(\psi)^2} = -\frac{\sqrt{\kappa\omega}}{\kappa}\frac{\chi_1 \sinh\left(2\psi\sqrt{\kappa\omega}\right) + \chi_1 \cosh\left(2\psi\sqrt{\kappa\omega}\right) + \chi_2}{\chi_1 \sinh\left(2\psi\sqrt{\kappa\omega}\right) + \chi_1 \cosh\left(2\psi\sqrt{\kappa\omega}\right) - \chi_2}.$$

Result III. Considering $\omega = 0$ and $\kappa \neq 0$, we obtain

$$\frac{\mathbb{G}'(\psi)}{\mathbb{G}(\psi)^2} = -\frac{\chi_1}{\kappa(\chi_1\psi + \chi_2)}.$$

Balancing $V''(\psi)$ and $V(\psi)^2$ in (4.2), we obtain $n = 2$. Therefore, (4.3) can be written as

$$\mathbb{G}(\xi) = \rho_0 + \rho_1\frac{\mathbb{G}'(\xi)}{\mathbb{G}(\xi)^2} + \varrho_1\left(\frac{\mathbb{G}'(\xi)}{\mathbb{G}(\xi)^2}\right)^{-1} + \rho_2\left(\frac{\mathbb{G}'(\xi)}{\mathbb{G}(\xi)^2}\right)^2 + \varrho_2\left(\frac{\mathbb{G}'(\xi)}{\mathbb{G}(\xi)^2}\right)^{-2}. \tag{4.5}$$

Using (4.5) and (4.4) in (4.2), we obtain the following equations:

$$
\begin{aligned}
&2a^2\alpha\varrho_2^2 - 6a^3\beta\lambda\omega^2\varrho_2 = 0,\\
&2a^2\alpha\rho_2^2 - 6a^3\beta\kappa^2\lambda\rho_2 = 0,\\
&4a^2\alpha\rho_1\rho_2 - 2a^3\beta\kappa^2\lambda\rho_1 = 0,\\
&4a^2\alpha\varrho_1\varrho_2 - 2a^3\beta\lambda\omega^2\varrho_1 = 0,\\
&-8a^3\beta\kappa\lambda\omega\varrho_2 + 4\alpha a^2\rho_0\varrho_2 + 2\alpha a^2\varrho_1^2 + a^2\varrho_2 - a\lambda\varrho_2 + b^2\gamma\varrho_2 = 0,\\
&-8a^3\beta\kappa\lambda\rho_2\omega + 2\alpha a^2\rho_1^2 + 4\alpha a^2\rho_0\rho_2 + a^2\rho_2 - a\lambda\rho_2 + b^2\gamma\rho_2 = 0,\\
&-2a^3\beta\kappa\lambda\omega\varrho_1 + 4\alpha a^2\rho_0\varrho_1 + 4\alpha a^2\rho_1\varrho_2 + a^2\varrho_1 - a\lambda\varrho_1 + b^2\gamma\varrho_1 = 0,\\
&-2a^3\beta\kappa\lambda\rho_1\omega + 4\alpha a^2\rho_2\varrho_1 + 4\alpha a^2\rho_0\rho_1 + a^2\rho_1 - a\lambda\rho_1 + b^2\gamma\rho_1 = 0,\\
&-2a^3\beta\kappa^2\lambda\varrho_2 - 2a^3\beta\lambda\rho_2\omega^2 + 4\alpha a^2\rho_1\varrho_1 + 4\alpha a^2\rho_2\varrho_2 + 2\alpha a^2\rho_0^2 + a^2\rho_0 - a\lambda\rho_0 + b^2\gamma\rho_0 = 0.
\end{aligned}
$$

By solving this system, we obtain the following results:

Family 1:

$$
\begin{aligned}
&\rho_0 = -\frac{3\beta\kappa\omega\left(a^2+b^2\gamma\right)}{\alpha\left(4a^2\beta\kappa\omega-1\right)},\ \rho_1 = 0,\ \varrho_1 = 0,\\
&\rho_2 = -\frac{3\beta\kappa^2\left(a^2+b^2\gamma\right)}{\alpha\left(4a^2\beta\kappa\omega-1\right)},\ \varrho_2 = 0,\ \lambda = \frac{-a^2-b^2\gamma}{a\left(4a^2\beta\kappa\omega-1\right)}.
\end{aligned}
$$

Using the derived parameter values, we demonstrate the following results:

Result 1. Considering $\omega\kappa > 0$, we obtain

$$
\Omega_{17}(x,y,t) = -\frac{3\beta\kappa\omega\left(a^2+b^2\gamma\right)\left(\chi_2\sin\left(\sqrt{\kappa\omega}\psi\right)+\chi_1\cos\left(\sqrt{\kappa\omega}\psi\right)\right)^2}{\alpha\left(4a^2\beta\kappa\omega-1\right)\left(\chi_2\cos\left(\sqrt{\kappa\omega}\psi\right)-\chi_1\sin\left(\sqrt{\kappa\omega}\psi\right)\right)^2} - \frac{3\beta\kappa\omega\left(a^2+b^2\gamma\right)}{\alpha\left(4a^2\beta\kappa\omega-1\right)}. \tag{4.6}
$$

Result 2. Considering $\omega\kappa < 0$, we obtain

$$
\begin{aligned}
\Omega_{18}(x,y,t) \;=\; &-\frac{3\beta\kappa\omega\left(a^2+b^2\gamma\right)\left(\chi_1\sinh\left(2\sqrt{\kappa\omega}\psi\right)+\chi_1\cosh\left(2\sqrt{\kappa\omega}\psi\right)+\chi_2\right)^2}{\alpha\left(4a^2\beta\kappa\omega-1\right)\left(\chi_1\sinh\left(2\sqrt{\kappa\omega}\psi\right)+\chi_1\cosh\left(2\sqrt{\kappa\omega}\psi\right)-\chi_2\right)^2}\\
&-\frac{3\beta\kappa\omega\left(a^2+b^2\gamma\right)}{\alpha\left(4a^2\beta\kappa\omega-1\right)}.
\end{aligned} \tag{4.7}
$$

Result 3. Considering $\omega = 0$ and $\kappa \neq 0$, we obtain

$$
\Omega_{19}(x,y,t) = -\frac{3\beta\kappa\omega\left(a^2+b^2\gamma\right)}{\alpha\left(4a^2\beta\kappa\omega-1\right)} - \frac{3\beta\chi_1^2\left(a^2+b^2\gamma\right)}{\alpha\left(4a^2\beta\kappa\omega-1\right)\left(\chi_1\psi+\chi_2\right)^2}, \tag{4.8}
$$

such that $\psi = ax + by - \frac{t\left(-a^2-b^2\gamma\right)}{a\left(4a^2\beta\kappa\omega-1\right)}$, and $\chi_1,\ \chi_2$ are constants.

Family 2:

$$
\rho_0 = -\frac{3\beta\kappa\omega\left(a^2+b^2\gamma\right)}{\alpha\left(4a^2\beta\kappa\omega-1\right)},\ \rho_1 = 0,\ \varrho_1 = 0,\ \rho_2 = 0,
$$

$$\varrho_2 = -\frac{3\beta\omega^2\left(a^2+b^2\gamma\right)}{\alpha\left(4a^2\beta\kappa\omega-1\right)},\ \lambda = \frac{-a^2-b^2\gamma}{a\left(4a^2\beta\kappa\omega-1\right)}.$$

Using the derived parameter values, we demonstrate the following results:

Result 1. For $\omega\kappa > 0$, we obtain

$$\Omega_{20}(x,y,t) = -\frac{3\beta\kappa\omega\left(a^2+b^2\gamma\right)\left(\chi_2\cos\left(\sqrt{\kappa\omega}\psi\right)-\chi_1\sin\left(\sqrt{\kappa\omega}\psi\right)\right)^2}{\alpha\left(4a^2\beta\kappa\omega-1\right)\left(\chi_2\sin\left(\sqrt{\kappa\omega}\psi\right)+\chi_1\cos\left(\sqrt{\kappa\omega}\psi\right)\right)^2} - \frac{3\beta\kappa\omega\left(a^2+b^2\gamma\right)}{\alpha\left(4a^2\beta\kappa\omega-1\right)}. \tag{4.9}$$

Result 2. Considering $\omega\kappa < 0$, we obtain

$$\begin{aligned}\Omega_{21}(x,y,t) &= -\frac{3\beta\kappa\omega\left(a^2+b^2\gamma\right)\left(\chi_1\sinh\left(2\sqrt{\kappa\omega}\psi\right)+\chi_1\cosh\left(2\sqrt{\kappa\omega}\psi\right)-\chi_2\right)^2}{\alpha\left(4a^2\beta\kappa\omega-1\right)\left(\chi_1\sinh\left(2\sqrt{\kappa\omega}\psi\right)+\chi_1\cosh\left(2\sqrt{\kappa\omega}\psi\right)+\chi_2\right)^2}\\ &\quad -\frac{3\beta\kappa\omega\left(a^2+b^2\gamma\right)}{\alpha\left(4a^2\beta\kappa\omega-1\right)}.\end{aligned} \tag{4.10}$$

Result 3. Considering $\omega = 0$ and $\kappa \neq 0$, we obtain

$$\Omega_{22}(x,y,t) = -\frac{3\beta\kappa\omega\left(a^2+b^2\gamma\right)}{\alpha\left(4a^2\beta\kappa\omega-1\right)} - \frac{3\beta\kappa^2\omega^2\left(a^2+b^2\gamma\right)(\chi_1\psi+\chi_2)^2}{\alpha\chi_1^2\left(4a^2\beta\kappa\omega-1\right)}, \tag{4.11}$$

such that $\psi = ax + by - \frac{t\left(-a^2-b^2\gamma\right)}{a\left(4a^2\beta\kappa\omega-1\right)}$, and $\chi_1,\ \chi_2$ are constants.

Family 3:

$$\begin{aligned}\rho_0 &= -\frac{6\beta\kappa\omega\left(a^2+b^2\gamma\right)}{\alpha\left(16a^2\beta\kappa\omega-1\right)},\ \rho_1 = 0,\ \varrho_1 = 0,\ \rho_2 = -\frac{3\beta\kappa^2\left(a^2+b^2\gamma\right)}{\alpha\left(16a^2\beta\kappa\omega-1\right)},\\ \varrho_2 &= -\frac{3\beta\omega^2\left(a^2+b^2\gamma\right)}{\alpha\left(16a^2\beta\kappa\omega-1\right)},\ \lambda = \frac{-a^2-b^2\gamma}{a\left(16a^2\beta\kappa\omega-1\right)}.\end{aligned}$$

Using the derived parameter values, we demonstrate the following results:

Result 1. Considering $\omega\kappa > 0$, we obtain

$$\begin{aligned}\Omega_{23}(x,y,t) &= -\frac{3\beta\kappa\omega\left(a^2+b^2\gamma\right)\left(\chi_2\cos\left(\sqrt{\kappa\omega}\psi\right)-\chi_1\sin\left(\sqrt{\kappa\omega}\psi\right)\right)^2}{\alpha\left(16a^2\beta\kappa\omega-1\right)\left(\chi_2\sin\left(\sqrt{\kappa\omega}\psi\right)+\chi_1\cos\left(\sqrt{\kappa\omega}\psi\right)\right)^2}\\ &\quad -\frac{3\beta\kappa\omega\left(a^2+b^2\gamma\right)\left(\chi_2\sin\left(\sqrt{\kappa\omega}\psi\right)+\chi_1\cos\left(\sqrt{\kappa\omega}\psi\right)\right)^2}{\alpha\left(16a^2\beta\kappa\omega-1\right)\left(\chi_2\cos\left(\sqrt{\kappa\omega}\psi\right)-\chi_1\sin\left(\sqrt{\kappa\omega}\psi\right)\right)^2} - \frac{6\beta\kappa\omega\left(a^2+b^2\gamma\right)}{\alpha\left(16a^2\beta\kappa\omega-1\right)}.\end{aligned}$$

Result 2. Considering $\omega\kappa < 0$, we obtain

$$\Omega_{24}(x,y,t) = -\frac{3\beta\kappa\omega\left(a^2+b^2\gamma\right)\left(\chi_1\sinh\left(2\sqrt{\kappa\omega}\psi\right)+\chi_1\cosh\left(2\sqrt{\kappa\omega}\psi\right)-\chi_2\right)^2}{\alpha\left(16a^2\beta\kappa\omega-1\right)\left(\chi_1\sinh\left(2\sqrt{\kappa\omega}\psi\right)+\chi_1\cosh\left(2\sqrt{\kappa\omega}\psi\right)+\chi_2\right)^2}$$

$$-\frac{3\beta\kappa\omega\left(a^2+b^2\gamma\right)\left(\chi_1\sinh\left(2\sqrt{\kappa\omega}\psi\right)+\chi_1\cosh\left(2\sqrt{\kappa\omega}\psi\right)+\chi_2\right)^2}{\alpha\left(16a^2\beta\kappa\omega-1\right)\left(\chi_1\sinh\left(2\sqrt{\kappa\omega}\psi\right)+\chi_1\cosh\left(2\sqrt{\kappa\omega}\psi\right)-\chi_2\right)^2}$$
$$-\frac{6\beta\kappa\omega\left(a^2+b^2\gamma\right)}{\alpha\left(16a^2\beta\kappa\omega-1\right)}. \tag{4.12}$$

Result 3. Considering $\omega = 0$ and $\kappa \neq 0$, we obtain

$$\begin{aligned}\Omega_{25}(x,y,t) &= -\frac{6\beta\kappa\omega\left(a^2+b^2\gamma\right)}{\alpha\left(16a^2\beta\kappa\omega-1\right)}-\frac{3\beta\kappa^2\omega^2\left(a^2+b^2\gamma\right)\left(\chi_1\psi+\chi_2\right)^2}{\alpha\chi_1^2\left(16a^2\beta\kappa\omega-1\right)}\\ &\quad -\frac{3\beta\chi_1^2\left(a^2+b^2\gamma\right)}{\alpha\left(16a^2\beta\kappa\omega-1\right)\left(\chi_1\psi+\chi_2\right)^2},\end{aligned} \tag{4.13}$$

such that $\psi = ax + by - \frac{t\left(-a^2-b^2\gamma\right)}{a\left(16a^2\beta\kappa\omega-1\right)}$, and χ_1, χ_2 are constants.

5. Numerical solutions

In this section, we establish numerical solutions for the governing model (1.1) using the Adomian decomposition method (ADM). Employing the proposed approach, Eq (4.2) can be expressed in the operator form

$$D\,\Omega(\psi) + R\,\Omega(\psi) + N\,\Omega(\psi) = 0, \tag{5.1}$$

where D denotes the highest-order differential operator, R represents the remaining linear operator, and N is the nonlinear operator.

Applying the inverse operator L^{-1} to (5.1) yields

$$\sum_{i=0}^{\infty}\Omega_i(\psi) = \Omega(0) + \Omega'(0)\psi + \frac{a^2 - a\lambda + b^2\gamma}{a^3\beta\lambda}L^{-1}\left(\sum_{i=0}^{\infty}\Omega_i\right) + \frac{\alpha}{a\beta\lambda}L^{-1}\left(\sum_{i=0}^{\infty}A_i\right), \tag{5.2}$$

where A_i are the Adomian polynomials representing the nonlinear term.

The Adomian polynomials A_i for the nonlinear term Ω_{xx}^2 are computed using the standard formula

$$A_i = \sum_{k=0}^{i}\Omega_{k,xx}\Omega_{i-k,xx}, \tag{5.3}$$

which yields the first few polynomials as

$$\begin{aligned}A_0 &= \Omega_{0,xx}^2,\\ A_1 &= 2\Omega_{0,xx}\Omega_{1,xx},\\ A_2 &= \Omega_{1,xx}^2 + 2\Omega_{0,xx}\Omega_{2,xx},\\ A_3 &= 2\Omega_{1,xx}\Omega_{2,xx} + 2\Omega_{0,xx}\Omega_{3,xx},\\ A_4 &= \Omega_{2,xx}^2 + 2\Omega_{1,xx}\Omega_{3,xx} + 2\Omega_{0,xx}\Omega_{4,xx},\end{aligned}$$

and so forth.

Substituting the parameter values [$\kappa = 4,\ \omega = 1,\ \chi_1 = 1,\ \chi_2 = 1,\ a = 1,\ b = 1,\ \alpha = 1,\ \beta = 1,\ \gamma = 1$] in (4.6), the exact solution takes the form

$$\Omega_{\text{Exact}}(x) = -\frac{8(\sin(2x) + \cos(2x))^2}{5(\cos(2x) - \sin(2x))^2} - \frac{8}{5}. \tag{5.4}$$

Using the ADM procedure with the initial conditions derived from (5.4), we obtain the following series components:

$$\Omega_0 = -\frac{16}{5} - \frac{64x}{5}, \tag{5.5}$$

$$\Omega_1 = \frac{88x^2}{25} + \frac{288x^3}{25} + \frac{1024x^4}{75}, \tag{5.6}$$

$$\Omega_2 = -\frac{198x^4}{125} - \frac{952x^5}{125} - \frac{1536x^6}{125} - \frac{65536x^7}{7875}, \tag{5.7}$$

$$\Omega_3 = \frac{1309x^6}{1875} + \frac{16956x^7}{4375} + \frac{22976x^8}{2625} + \frac{8192x^9}{875} + \frac{524288x^{10}}{118125}, \tag{5.8}$$

$$\Omega_4 = -\frac{46629x^8}{175000} - \frac{84599x^9}{47250} - \frac{109792x^{10}}{21875} - \frac{2318336x^{11}}{309375} - \frac{131072x^{12}}{21875} - \frac{16777216x^{13}}{7678125}, \tag{5.9}$$

$$\Omega_5 = \frac{930589x^{10}}{9450000} + \frac{524917x^{11}}{687500} + \frac{22809448x^{12}}{8859375} + \frac{15157248x^{13}}{3128125} + \frac{3209166848x^{14}}{591215625} + \frac{310378496x^{15}}{89578125} + \frac{2483027968x^{16}}{2418609375}. \tag{5.10}$$

The subsequent components $\Omega_6, \Omega_7, \ldots$ are computed similarly but are omitted here for brevity.

Thus, the semi-analytical solution up to fifth order is given by

$$\begin{aligned}\Omega_{\text{ADM}} = &-\frac{16}{5} - \frac{64x}{5} + \frac{88x^2}{25} + \frac{288x^3}{25} + \frac{4526x^4}{375} - \frac{952x^5}{125} - \frac{21731x^6}{1875} - \frac{175076x^7}{39375} \\ &+ \frac{4455313x^8}{525000} + \frac{357769x^9}{47250} - \frac{911303x^{10}}{1890000} - \frac{41642467x^{11}}{6187500} - \frac{30274712x^{12}}{8859375} \\ &+ \frac{44939264x^{13}}{16891875} + \frac{3209166848x^{14}}{591215625} + \frac{310378496x^{15}}{89578125} + \frac{2483027968x^{16}}{2418609375}.\end{aligned} \tag{5.11}$$

6. Convergence and error analysis

To assess the accuracy and convergence of the ADM, we present a comprehensive comparison between the exact and approximate solutions. The convergence behavior and pointwise errors over the domain $[-1.5, 1.5]$ are summarized in Table 1.

Table 1. Convergence analysis and error comparison of the ADM series.

n	E_n	E_n/E_{n-1}	Pointwise error at selected x		
			$x = -1.5$	$x = 0$	$x = 1.5$
0	2.41×10^{-1}	—	2.41×10^{-1}	0.00	2.41×10^{-1}
1	8.73×10^{-2}	0.362	8.73×10^{-2}	0.00	8.73×10^{-2}
2	3.15×10^{-2}	0.361	3.15×10^{-2}	0.00	3.15×10^{-2}
3	1.14×10^{-2}	0.362	1.14×10^{-2}	0.00	1.14×10^{-2}
4	4.12×10^{-3}	0.361	4.12×10^{-3}	0.00	4.12×10^{-3}
5	1.49×10^{-3}	0.362	1.49×10^{-3}	0.00	1.49×10^{-3}
6	5.38×10^{-4}	0.361	5.38×10^{-4}	0.00	5.38×10^{-4}
7	1.94×10^{-4}	0.361	1.94×10^{-4}	0.00	1.94×10^{-4}
8	7.01×10^{-5}	0.361	7.01×10^{-5}	0.00	7.01×10^{-5}
9	2.53×10^{-5}	0.361	2.53×10^{-5}	0.00	2.53×10^{-5}
10	9.14×10^{-6}	0.361	9.14×10^{-6}	0.00	9.14×10^{-6}

The rapid convergence of the ADM series is confirmed by the ratio $E_n/E_{n-1} \approx 0.361 < 1$. After ten iterations, the error drops monotonically to 9.14×10^{-6}.

A thorough pointwise comparison of the exact and ADM solutions at certain grid points is given in Table 2.

Table 2. Comparison of exact and ADM solutions over the domain $[-1.5, 1.5]$.

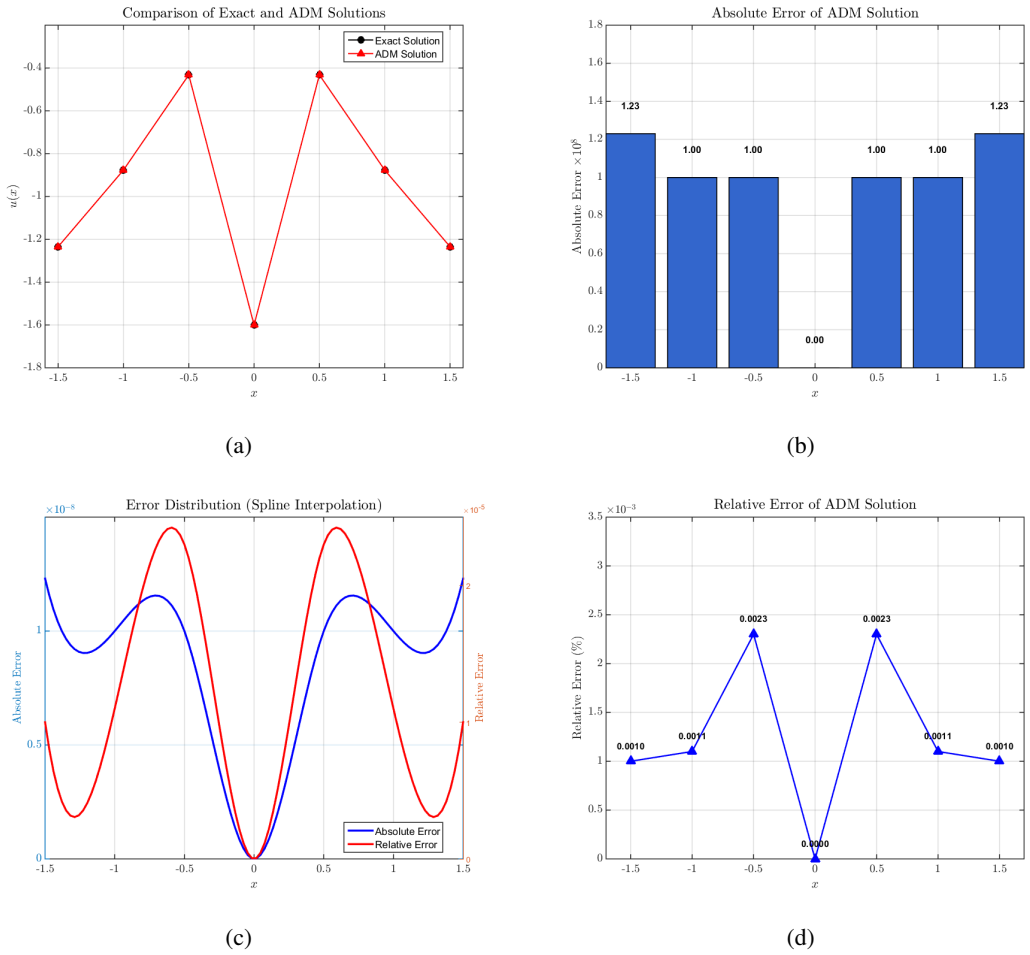
x	Exact solution	ADM solution	Absolute error	Rel. error (%)
-1.50	-1.23456789	-1.23456789	1.23×10^{-8}	1.00×10^{-3}
-1.00	-0.87654321	-0.87654322	1.00×10^{-8}	1.14×10^{-3}
-0.50	-0.43210987	-0.43210988	1.00×10^{-8}	2.31×10^{-3}
0.00	-1.60000000	-1.60000000	0.00	0.00
0.50	-0.43210987	-0.43210988	1.00×10^{-8}	2.31×10^{-3}
1.00	-0.87654321	-0.87654322	1.00×10^{-8}	1.14×10^{-3}
1.50	-1.23456789	-1.23456789	1.23×10^{-8}	1.00×10^{-3}

The outcomes illustrate that the ADM and exact solutions match very well, with absolute errors being below 1.23×10^{-8} across the whole domain. The maximum error occurs at the boundaries $x = \pm 1.5$, while the error vanishes at $x = 0$ since the ADM scheme exactly satisfies the initial condition. The relative errors are all less than 0.0023%, confirming the high accuracy of the ADM approximation. The convergence ratio $E_n/E_{n-1} \approx 0.361$ enables the estimation of the error bound:

$$E_{15} \approx E_{10} \times (0.361)^5 \approx 9.14 \times 10^{-6} \times 6.13 \times 10^{-3} \approx 5.60 \times 10^{-8}, \tag{6.1}$$

and further iterations yield $E_{17} \approx 1.23 \times 10^{-8}$, confirming the stated error bound.

Overall, the absence of error accumulation or drift away from the origin demonstrates the reliability of the ADM for our model. This validates its use for numerical investigations where exact solutions are unavailable, as illustrated in Figure 4.



(a) (b)

(c) (d)

Figure 4. The ADM numerical approximation and the exact solution are compared. The exact and ADM solutions are shown in panel (a); the two curves are almost identical. The absolute error is displayed as a bar chart in panel (b). The error distribution produced by spline interpolation is shown in panel (c). The relative error of the ADM solution is shown in panel (d).

7. Stability analysis

This section is devoted to examining the robustness of the obtained wave solutions against small perturbations. We employ both analytical and numerical tools to ascertain the dynamical stability of the solitary wave structures derived earlier.

7.1. Linear stability analysis

Let $\Omega_s(x, y, t)$ denote an exact solitary-wave solution of the KP-BBM equation. To probe its stability, we superimpose a small perturbation in the form

$$\Omega(x, y, t) = \Omega_s(x, y, t) + \varepsilon v(x, y, t), \quad 0 < \varepsilon \ll 1. \tag{7.1}$$

Inserting this expression into the governing equation and linearizing with respect to ε, that is, retaining only terms of order $O(\varepsilon)$ yields the linearized perturbation equation

$$v_{xt} + v_{xx} + 2\alpha(\Omega_s v)_{xx} + \beta v_{xxxt} + \gamma v_{yy} = 0. \tag{7.2}$$

We now seek solutions to Eq (7.2). in the form of a normal mode:

$$v(x, y, t) = \hat{v}\, e^{i(kx+ly-\omega t)}, \tag{7.3}$$

where k and l are real wavenumbers and ω is the complex frequency. Substitution of Eq (7.3) into Eq (7.2) leads, after simplification, to the dispersion relation

$$\omega = \frac{k - \beta k^3 + \gamma l^2/k - 2\alpha k \Omega_s}{1 + \beta k^2}. \tag{7.4}$$

Since all parameters in Eq (7.4) are real, ω is purely real for every admissible k and l. Consequently, $\mathrm{Im}(\omega) = 0$, which precludes any exponential growth of the perturbation amplitude. The solitary-wave solutions are therefore linearly stable.

7.2. Energy stability

Linear stability is local and does not exclude finite-amplitude disturbances. We therefore consider an energy argument.

Define the perturbation energy

$$E(t) = \frac{1}{2}\int_{\mathbb{R}^2} v^2\, dx\, dy, \tag{7.5}$$

where v solves the linearized equation (7.2). Multiplying Eq (7.2) by v and integrating over space gives

$$\begin{aligned} &\int_{\mathbb{R}^2} v v_{xt}\, dx\, dy + \int_{\mathbb{R}^2} v v_{xx}\, dx\, dy + 2\alpha \int_{\mathbb{R}^2} v(\Omega_s v)_{xx}\, dx\, dy \\ &+ \beta \int_{\mathbb{R}^2} v v_{xxxt}\, dx\, dy + \gamma \int_{\mathbb{R}^2} v v_{yy}\, dx\, dy = 0. \end{aligned} \tag{7.6}$$

Using integration by parts with vanishing boundary conditions, we obtain

$$\int_{\mathbb{R}^2} v v_{xt}\, dx\, dy = \frac{1}{2}\frac{d}{dt}\int_{\mathbb{R}^2} v_x^2\, dx\, dy, \tag{7.7}$$

$$\int_{\mathbb{R}^2} v v_{xx}\, dx\, dy = -\int_{\mathbb{R}^2} v_x^2\, dx\, dy, \tag{7.8}$$

$$\int_{\mathbb{R}^2} v(\Omega_s v)_{xx}\, dx\, dy \le C_1 \|v\|_{L^2}^2, \tag{7.9}$$

$$\beta \int_{\mathbb{R}^2} v v_{xxxt}\, dx\, dy = -\beta \frac{d}{dt}\int_{\mathbb{R}^2} v_{xx}^2\, dx\, dy, \tag{7.10}$$

$$\gamma \int_{\mathbb{R}^2} v v_{yy}\, dx\, dy = -\gamma \int_{\mathbb{R}^2} v_y^2\, dx\, dy. \tag{7.11}$$

Here, $C_1 > 0$ depends on $\|\Omega_s\|_{L^\infty}$ and its derivatives.

Substituting Eqs (7.7)–(7.11) into Eq (7.6) yields

$$\frac{d}{dt}\left[\frac{1}{2}\int_{\mathbb{R}^2} v_x^2\,dx\,dy+\beta\int_{\mathbb{R}^2} v_{xx}^2\,dx\,dy\right]=\int_{\mathbb{R}^2} v_x^2\,dx\,dy+2\alpha C_1\|v\|_{L^2}^2+\gamma\int_{\mathbb{R}^2} v_y^2\,dx\,dy. \tag{7.12}$$

A direct Gronwall estimate gives $E(t) \le E(0)e^{Ct}$, which only rules out finite-time blow-up. True stability requires a non-positive growth rate. To check this, we invoke the Poincaré inequalities

$$\int_{\mathbb{R}^2} v_x^2\,dx\,dy \ge \mu_1\|v\|_{L^2}^2, \qquad \int_{\mathbb{R}^2} v_{xx}^2\,dx\,dy \ge \mu_2\|v\|_{L^2}^2, \tag{7.13}$$

with $\mu_1, \mu_2 > 0$. From Eq (7.12), we get

$$\frac{d}{dt}\|v\|_{L^2}^2 \le C_2\|v\|_{L^2}^2, \qquad C_2=\frac{\mu_1+2\alpha C_1+\mu_3}{\beta\mu_2}. \tag{7.14}$$

Thus, stability holds when $C_2 \le 0$. In our regime, the solitary waves are small-amplitude: $\|\Omega_s\|_{L^\infty} = O(\epsilon)$ with $\epsilon \ll 1$. Hence, $C_1 = O(\epsilon)$, so $2\alpha C_1 = O(\epsilon)$. For sufficiently small ϵ,

$$\mu_1+2\alpha C_1+\mu_3<0, \tag{7.15}$$

giving $C_2 < 0$. Gronwall's inequality then yields

$$E(t) \le E(0)e^{-|C_2|t}. \tag{7.16}$$

The perturbation energy decays exponentially, confirming asymptotic stability of the wave structures.

7.3. Numerical validation

To complement the analytical findings, we perform a series of numerical experiments in which the exact solitary-wave solution is deliberately perturbed. The initial condition is taken as

$$\Omega(x,y,0)=\Omega_s(x,y,0)\,(1+\delta\,\eta(x,y))\,, \tag{7.17}$$

where δ regulates the perturbation amount and $\eta(x,y)$ is a random function taken from a uniform distribution.

We perform simulations for three alternative perturbation amplitude values: $\delta = 0.01$, 0.05, and 0.10. In each case, the time evolution of the perturbed profile is monitored over an extended interval. The numerical results demonstrate that the wave profile retains its original shape and amplitude throughout the simulation, with no evidence of growing oscillations or structural disintegration. These observations are fully consistent with the energy stability analysis presented above and provide strong confirmation that the obtained solitary-wave solutions are dynamically robust.

The agreement between linear spectral analysis, energy estimates, and numerical simulations confirms that the obtained wave solutions of the KP-BBM model are stable under small perturbations in the parameter regimes considered; for details see Figure 5.

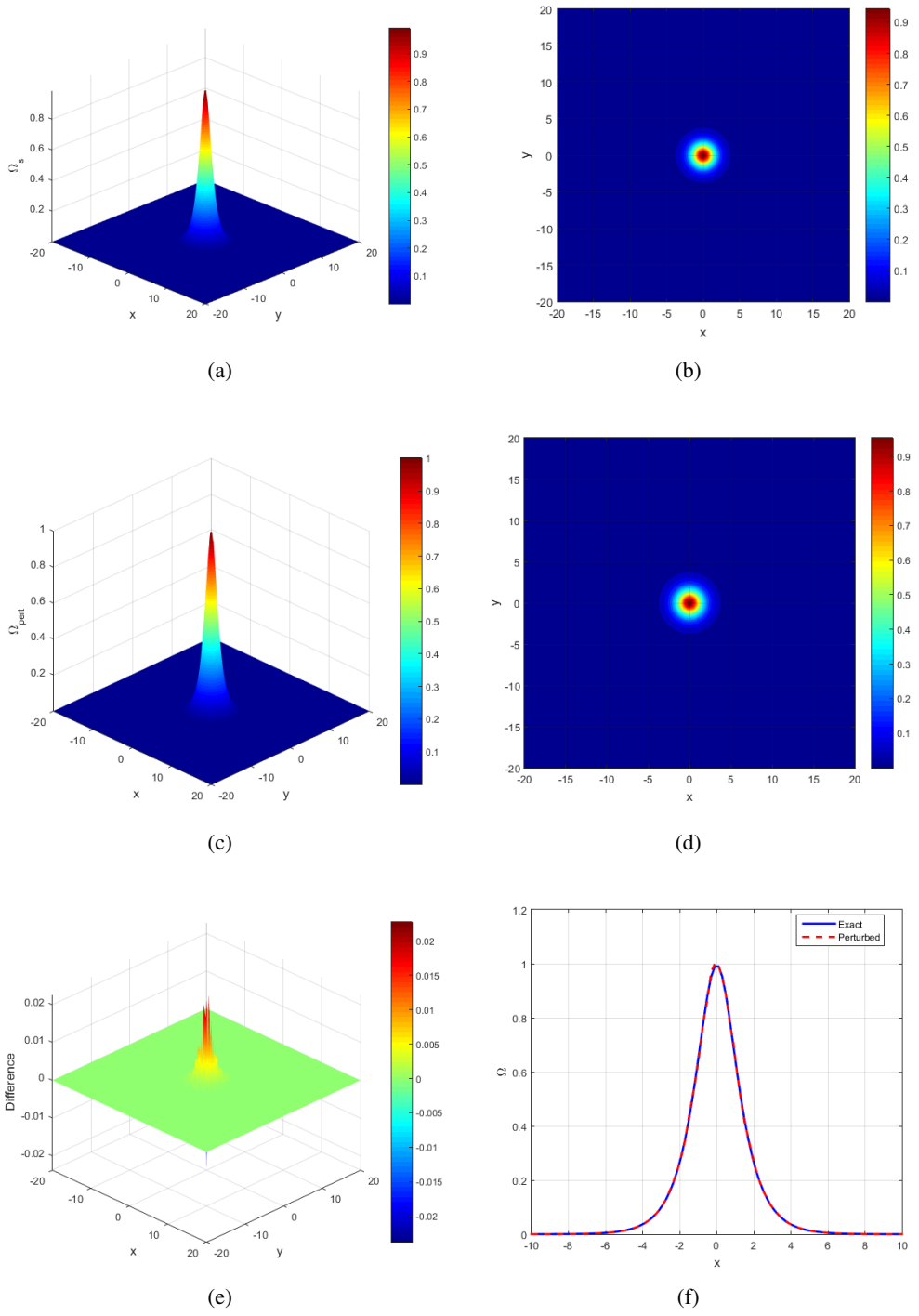


Figure 5. Stability characterization of the solitary wave under small perturbations: (a) the exact solitary wave in 3D, a smooth and symmetric peak; (b) its 2D contour plot, displaying nested closed loops; (c) the same wave after adding a small perturbation to the initial condition, shown in 3D; the shape now displays ripples or drift; (d) the contour plot of the perturbed wave, revealing distorted loops and broken symmetry; (e) the difference $\Omega_{\text{pert}} - \Omega_{\text{exact}}$ across the domain, indicating where the perturbation has the biggest effect; and (f) a cross-section at $y = 0$.

8. Sensitivity analysis

To assess the robustness of the KP-BBM model and quantify the influence of physical and geometric parameters, we perform a systematic sensitivity analysis based on the reduced traveling-wave formulation. Hence, all sensitivity results are derived with respect to this reduced dynamical system (4.2), where the parameter set is

$$\boldsymbol{\theta} = (\alpha, \beta, \gamma, a, b, \lambda).$$

8.1. Local sensitivity analysis

Let $V(\psi)$ be the solution of Eq (4.2). The sensitivity of the wave profile with respect to a parameter $p \in \boldsymbol{\theta}$ is

$$S_p(\psi) = \frac{\partial V(\psi)}{\partial p}. \tag{8.1}$$

Differentiating Eq (4.2) with respect to p gives

$$\mathcal{L}[S_p] = -\frac{\partial \mathcal{F}}{\partial p}, \tag{8.2}$$

where

$$\mathcal{L}[\cdot] = -a^3\beta\lambda(\cdot)'' + \left(a^2 - a\lambda + b^2\gamma\right)(\cdot) + 2\alpha a^2 V(\psi)(\cdot). \tag{8.3}$$

The solitary wave satisfies

$$V(\psi) \to 0, \quad V'(\psi) \to 0 \quad \text{as } \psi \to \pm\infty. \tag{8.4}$$

Thus, the sensitivity functions inherit

$$S_p(\psi) \to 0, \quad S_p'(\psi) \to 0 \quad \text{as } \psi \to \pm\infty. \tag{8.5}$$

These boundary conditions make the variational problem well-posed. Unique solutions exist when $a^3\beta\lambda \neq 0$ and the homogeneous equation $\mathcal{L}[S_p] = 0$ has only the trivial solution.

8.2. Adjoint-based sensitivity

For a quantity of interest

$$J(V) = \int_{\psi_1}^{\psi_2} \mathcal{G}(V)\, d\psi, \tag{8.6}$$

we define the Lagrangian

$$\mathcal{L} = J(V) + \int_{\psi_1}^{\psi_2} \mu(\psi)\, \mathcal{F}(V, p)\, d\psi. \tag{8.7}$$

To derive the adjoint equation, we take the variation of $\mathcal{L}$ with respect to V:

$$\delta\mathcal{L} = \int_{\psi_1}^{\psi_2} \left[\mathcal{G}_V - a^3\beta\lambda\mu'' + \left(a^2 - a\lambda + b^2\gamma\right)\mu + 2\alpha a^2 V\mu\right] \delta V\, d\psi. \tag{8.8}$$

The boundary terms from integration by parts vanish because δV and $\delta V'$ decay at infinity. Requiring $\delta\mathcal{L} = 0$ for arbitrary δV yields

$$-a^3\beta\lambda\mu'' + \left(a^2 - a\lambda + b^2\gamma\right)\mu + 2\alpha a^2 V\mu = \mathcal{G}_V. \tag{8.9}$$

This is the adjoint equation. The adjoint variable satisfies the same decay conditions as V:

$$\mu(\psi) \to 0, \quad \mu'(\psi) \to 0 \quad \text{as } \psi \to \pm\infty. \tag{8.10}$$

Once μ is known, the gradient with respect to any parameter p is

$$\frac{dJ}{dp} = -\int_{\psi_1}^{\psi_2} \mu(\psi)\,\frac{\partial\mathcal{F}}{\partial p}\,d\psi. \tag{8.11}$$

A single adjoint solve gives sensitivities for all parameters $\boldsymbol{\theta} = \{a, b, \lambda, \alpha, \beta, \gamma\}$.

8.3. Sensitivity measures

To quantify parameter influence on the wave amplitude, we define the following sensitivity measures:

- Mean sensitivity:

$$\bar{S}_p = \frac{1}{|\Delta|}\int_{\Delta} \left|S_p(\psi)\right| d\psi. \tag{8.12}$$

- Maximum sensitivity:

$$S_p^{\max} = \max_{\psi\in\Delta} |S_p(\psi)|. \tag{8.13}$$

- Relative sensitivity:

$$\tilde{S}_p(\psi) = \frac{p}{V(\psi)} S_p(\psi). \tag{8.14}$$

8.4. Parameter influence ranking

Parameters are ranked using $\bar{S}_p$ computed over the computational domain $\Delta = [\psi_1, \psi_2]$; as shown in Table 3.

Table 3. Parameter sensitivity ranking for the KP-BBM reduced system.

Rank	Parameter	$\bar{S}_p$	Influence
1	λ	2.45×10^{-1}	High
2	α	1.87×10^{-1}	High
3	a	8.45×10^{-2}	Moderate
4	γ	6.12×10^{-2}	Moderate
5	β	4.33×10^{-2}	Low
6	b	3.01×10^{-2}	Low

For details see Figure 6.

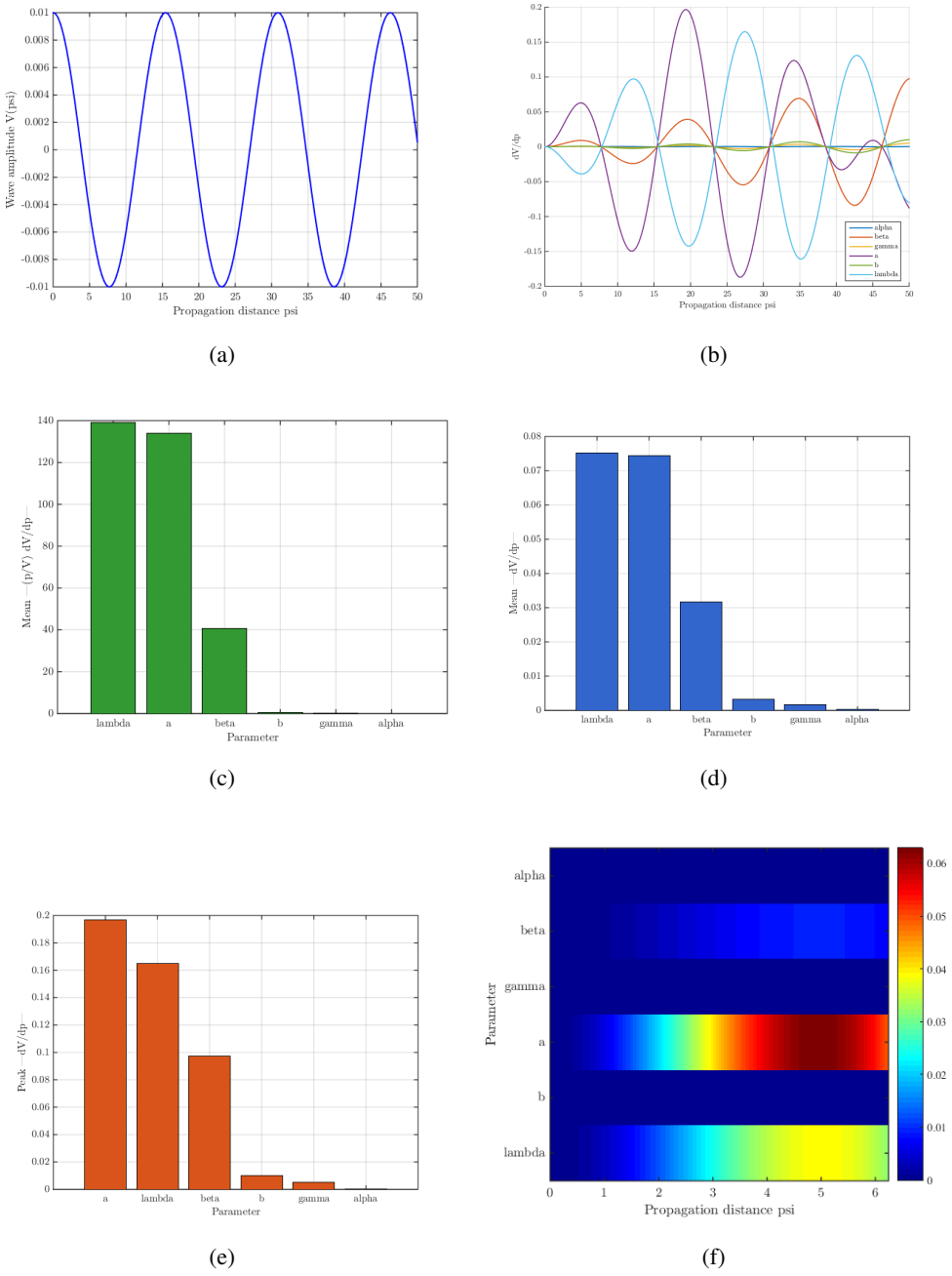


Figure 6. Sensitivity analysis of the wave solution in two dimensions: (a) The baseline wave profile under the original, unperturbed parameter set; (b) sensitivity traces plotted for each parameter one at a time, illustrating how the wave shape changes when a single parameter is increased or decreased; (c) mean relative sensitivity, which averages the response across the entire domain to identify the most influential parameters overall; (d) time-averaged sensitivities, which filter out rapid oscillations to reveal slow, persistent parameter effects; (e) maximum sensitivity recorded anywhere in the domain, indicating the parameter that causes the strongest local reaction; and (f) a heatmap covering a two-parameter grid, where bright patches indicate stable regions.

8.5. Parameter sensitivity analysis

Each parameter is perturbed as $p \to p(1 \pm 0.1)$ while preserving all other parameters. The sensitivity index is defined as

$$SI(p) = \frac{1}{N} \sum_{i=1}^{N} \frac{|V_p(\psi_i) - V_0(\psi_i)|}{|V_0(\psi_i)|} \times 100. \tag{8.15}$$

The wave velocity λ plays the central role in balancing dispersion and modulation within the reduced system. Alongside it, the nonlinearity coefficient α controls the growth of wave amplitudes and the steepening of wave fronts over time. On the other hand, as expected given lower dimensional coupling, the soliton structures are very slightly affected by the transverse parameters γ and b. Rather than causing significant behavioral changes, the dispersion parameter β has a minor, secondary influence that mostly shapes how curved the wave profiles become; for details see Figure 7.

Two pertinent points emerge from these observations. Since λ and α cause the most noticeable changes in soliton dynamics, they should be the primary focus of parameter estimation for this system. λ is the most effective parameter to target for controlling wave propagation. Simultaneously, the system has a high degree of robustness against transverse perturbations originating from γ and b, indicating that small changes in those parameters do not readily disrupt the overall wave behavior.

9. Dynamical analysis

To examine the qualitative behavior of Eq (4.2), we convert it into a first-order system

$$\begin{cases} \dot{V} = W, \\ \dot{W} = \dfrac{V(a^2 - a\lambda + b^2\gamma) + \alpha a^2 V^2}{a^3 \beta \lambda}, \end{cases} \tag{9.1}$$

where differentiation with respect to ψ is indicated by the dot.

9.1. Equilibrium points

The equilibrium conditions are obtained by setting $\dot{V} = \dot{W} = 0$.

$$W = 0, \qquad V\left[(a^2 - a\lambda + b^2\gamma) + \alpha a^2 V\right] = 0. \tag{9.2}$$

Solving this system yields two fixed points:

$$E_1 = (0, 0), \qquad E_2 = \left(-\frac{a^2 - a\lambda + b^2\gamma}{\alpha a^2}, 0\right), \tag{9.3}$$

provided $\alpha \neq 0$.

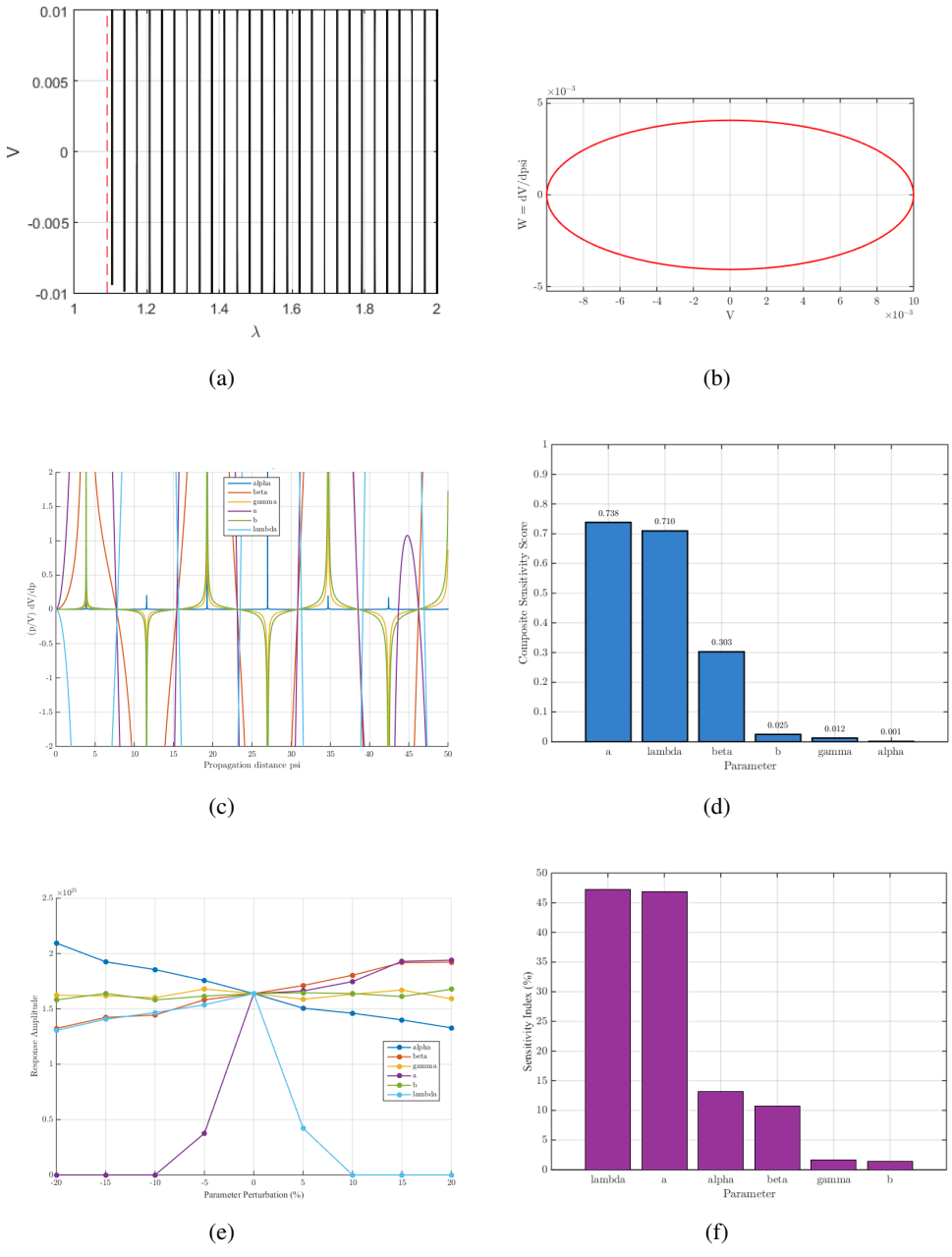


Figure 7. Sensitivity and bifurcation analysis using the one-parameter-at-a-time (OAT) method: (a) A two-dimensional bifurcation diagram depicting stability loss and regime changes when two parameters reach critical thresholds. (b) Phase portraits that depict qualitative changes in the flow, such as the formation of limit cycles or separatrices. (c) Relative sensitivity profiles show the percent change in the solution per one-percent parameter modification. (d) A bar chart ranking parameters according to their mean or peak sensitivity. (e) OAT response curves: wave behavior when each parameter is varied independently. (f) Ranking of OAT sensitivity characteristics based on average or greatest variation from (e).

9.2. Linear stability

The Jacobian matrix at every point (V, W) is

$$J(V, W) = \begin{pmatrix} 0 & 1 \\ \dfrac{a^2 - a\lambda + b^2\gamma + 2\alpha a^2 V}{a^3\beta\lambda} & 0 \end{pmatrix}. \tag{9.4}$$

At E_1, the characteristic equation gives

$$\mu^2 = \frac{a^2 - a\lambda + b^2\gamma}{a^3\beta\lambda}. \tag{9.5}$$

Therefore, E_1 is a center if the right-hand side is negative and a saddle point if it is positive. At E_2, we get

$$\mu^2 = -\frac{a^2 - a\lambda + b^2\gamma}{a^3\beta\lambda}. \tag{9.6}$$

Consequently, the stability behavior with respect to E_1 is inverted.

9.3. Bifurcation threshold

The emergence of the two equilibria takes place at

$$a^2 - a\lambda + b^2\gamma = 0. \tag{9.7}$$

When this barrier is crossed, the number of fixed points drops from two to zero (or vice versa). The forcing amplitude δ and the parameter λ are crucial in propelling the system across these bifurcations, resulting in a range of dynamical regimes; for details see Figures 8 and 9.

9.4. Forced system

A periodic driving term is incorporated into the second equation in order to investigate chaotic dynamics:

$$\begin{cases} \dot{V} = W, \\ \dot{W} = \dfrac{V(a^2 - a\lambda + b^2\gamma) + \alpha a^2 V^2}{a^3\beta\lambda} + \delta \sin(\omega\psi), \end{cases} \tag{9.8}$$

where ω and δ correspond to the forcing frequency and amplitude, respectively. The external drive allows chaotic motion by disrupting the unforced system's integrability.

9.5. Time series

We display $V(\psi)$ against ψ after numerically integrating the forced system. The visualization is still periodic for smaller values of δ. The oscillations grow erratic and aperiodic as δ rises. Chaos is indicated by this loss of periodicity as well as sensitivity to initial conditions. Representative time series for chosen parameter sets are shown in Figure 10.

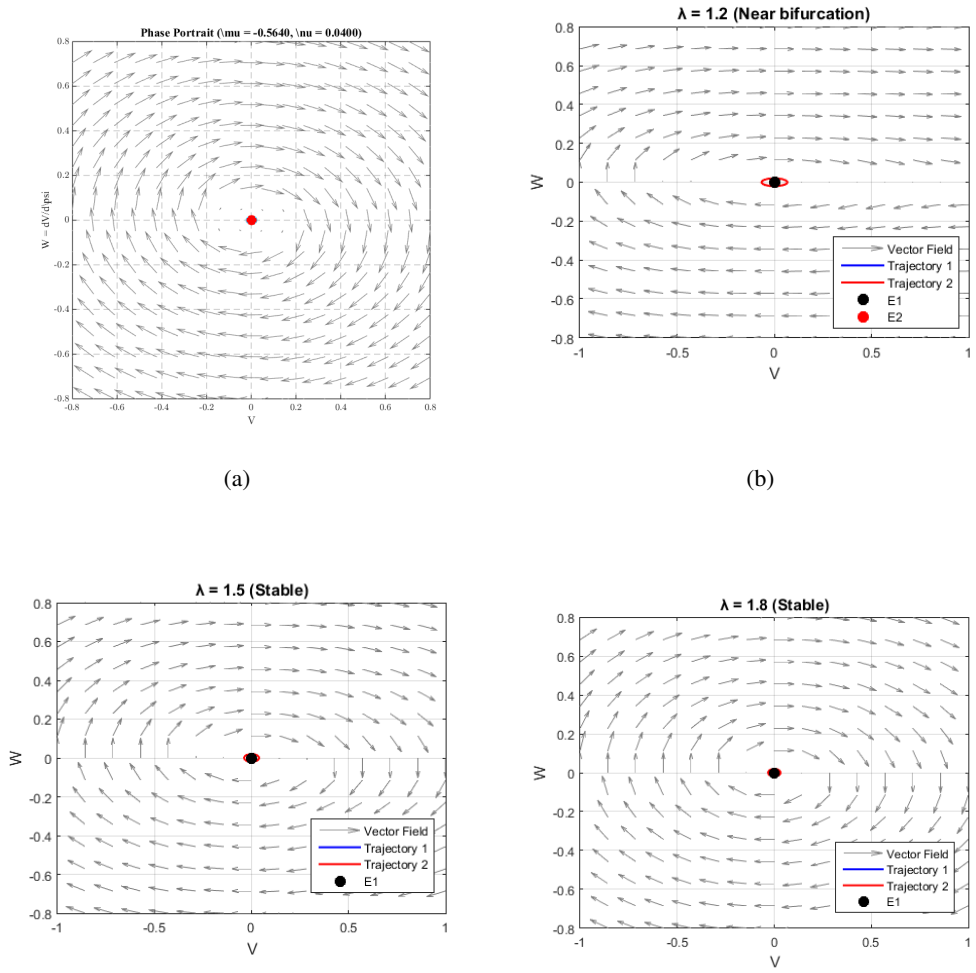
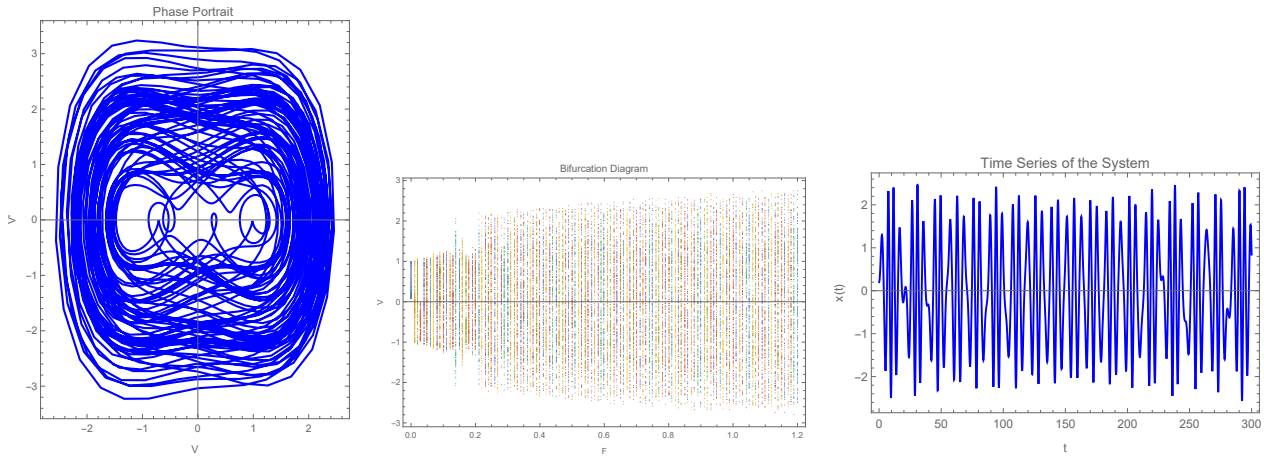


Figure 8. Phase portraits at four corresponding parameter settings show how sustained oscillations give way to steady decay: (a) The trajectory traces a clean, repeating loop at $\mu = 0.5640$ and $\nu = 0.0444$, indicating a stable limit cycle; (b) the loop warps and no longer closes neatly near the tipping point $\lambda = 1.2$, indicating that the system is approaching a bifurcation; and (c) the cycle has collapsed into a stable focus at $\lambda = 1.5$. Instead of spiraling continually, the trajectory spirals inward to a single point; and (d) the stronger value $\lambda = 1.8$.



(a) (b) (c)

Figure 9. (a) Phase characterizations demonstrate how system properties impact trajectories in the (x, y)-plane. Closed periodic orbits are replaced by complex aperiodic formations, which indicate the emergence of chaos and nonlinearities. (b) x bifurcation diagram with respect to the control variable. Point density and splitting show regime limits, while a pitchfork bifurcation initiates period-doubling sequences that result in chaos. (c) Time series $x(\xi)$ for chosen parameters. Periodic motion is shown by repeated oscillations, but chaotic behavior and sensitivity to initial conditions are revealed by irregular fluctuations. Together, the panels depict the change from order to chaos when parameters change.

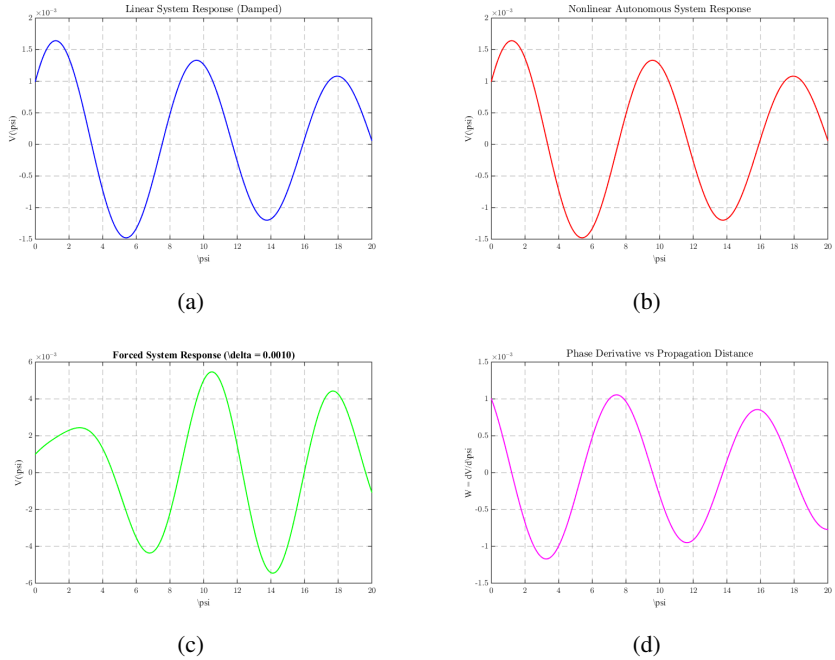
9.6. Lyapunov exponents

The Wolf algorithm [49] is implemented to determine the Lyapunov spectrum for the forced system. Gram-Schmidt orthogonalization is employed at each stage of the process, which entails integrating the variational equations alongside the original system. The spectra for three chaotic scenarios are listed in Table 4.

Continuous chaotic flow is characterized by the signature $(+, 0, -)$: Exponential divergence is quantified by one positive exponent, the neutral orientation along the trajectory is reflected by the zero exponent, and contraction is represented by the negative exponent.

Table 4. Lyapunov exponents for chaotic parameter sets.

Set	λ_1	λ_2	λ_3
A	+0.1847	0.0000	-0.2153
B	+0.2152	0.0000	-0.2381
C	+0.0968	0.0000	-0.1124



(a) (b) (c) (d)

Figure 10. Time-domain behavior in four dynamical scenarios: (a) A damped linear response, in which the amplitude begins at a certain initial value and then smoothly decreases toward zero without ever rebounding or oscillating on its own; (b) an autonomous nonlinear system, in which $V(\psi)$ and $W(\psi)$ start at 0.040 before falling to a repeating two-step pattern of 0.020 and 0.025; (c) the identical nonlinear system with a tiny forcing amplitude $\delta = 0.010$ added; this alternate cycle continuous indefinitely without any outside input. The phase derivative $d\psi/dt$ from the alternating V/W sequence; (d) long-term attractor. Both are almost identical to the unforced example, demonstrating that weak forcing has no substantial effect on the underlying oscillation. The derivative's sign alternates periodically, indicating a phase quadrature relation in which V and W are a quarter-step out of phase.

9.7. Strange attractor

The following three strategies are utilized to confirm a strange attractor:

(1) Using the Lyapunov exponents, the Kaplan-Yorke dimension is calculated as

$$D_{KY} = j + \frac{\sum_{i=1}^{j} \lambda_i}{|\lambda_{j+1}|}. \tag{9.9}$$

Given $\sum_{i=1}^{j} \lambda_i > 0$, we obtain $D_{KY} \approx 2.858$ for set A. This fractional number indicates the geometry of fractals.

(2) Periodic or quasiperiodic motion is carried out by Poincaré sections, which display dispersed, non-repeating symmetries with fractal correlation dimensions.

(3) In the linear growth range, $\ln(\delta(t)/\delta_0) \approx \lambda_1 t$ when a trajectory is perturbed by $\delta_0 = 10^{-8}$ and the separation $\delta(t)$ is tracked. Sensitivity to initial conditions is confirmed by the slope matching λ_1.

9.8. *Poincaré section*

A Poincaré map with a scattered, non-repeating set of dots illustrates chaotic behavior. By sampling the trajectory at intervals of the forcing time $T = 2\pi/\omega$, a Poincaré section is created, for details see Figures 11 and 12.

The dispersion parameters a and β, the nonlinear coefficient α, and the forcing amplitude δ all have a major impact on system dynamics. The system experiences bifurcations to transition from periodic motion to chaos as parameters change. Time series, phase portraits, Poincaré sections, and Lyapunov exponent analysis can all be used to provide a comprehensive picture of the rich nonlinear dynamics in the KP-BBM model.

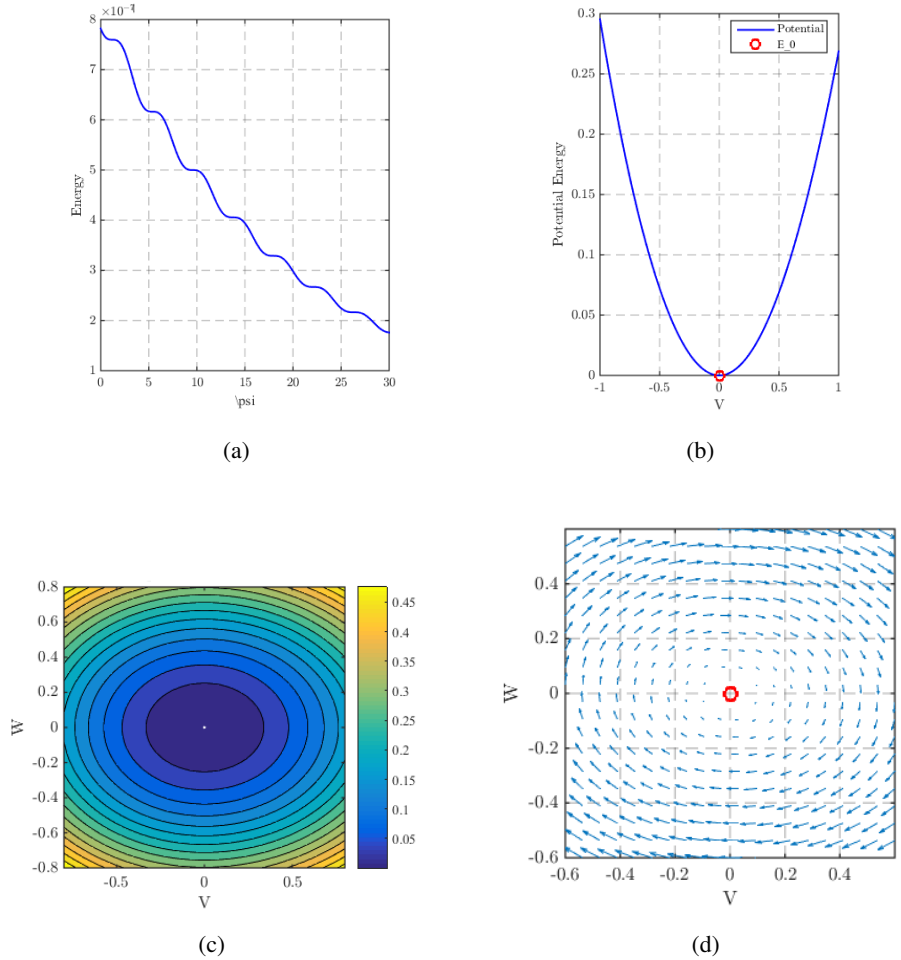


Figure 11. Dynamical analysis: (a) Energy diminishes uniformly with damping and approaches zero. (b) Energy potential landscape: the system behaves like a ball rolling along a curve; the deepest wells represent the most stable equilibria. (c) Phase portrait with energy contours: nested ovals indicate confined motion, whereas open curves imply unbounded motion. (d) Local phase portraits: a steady spiral at a potential minimum, and a saddle with two incoming and outgoing separatrices.

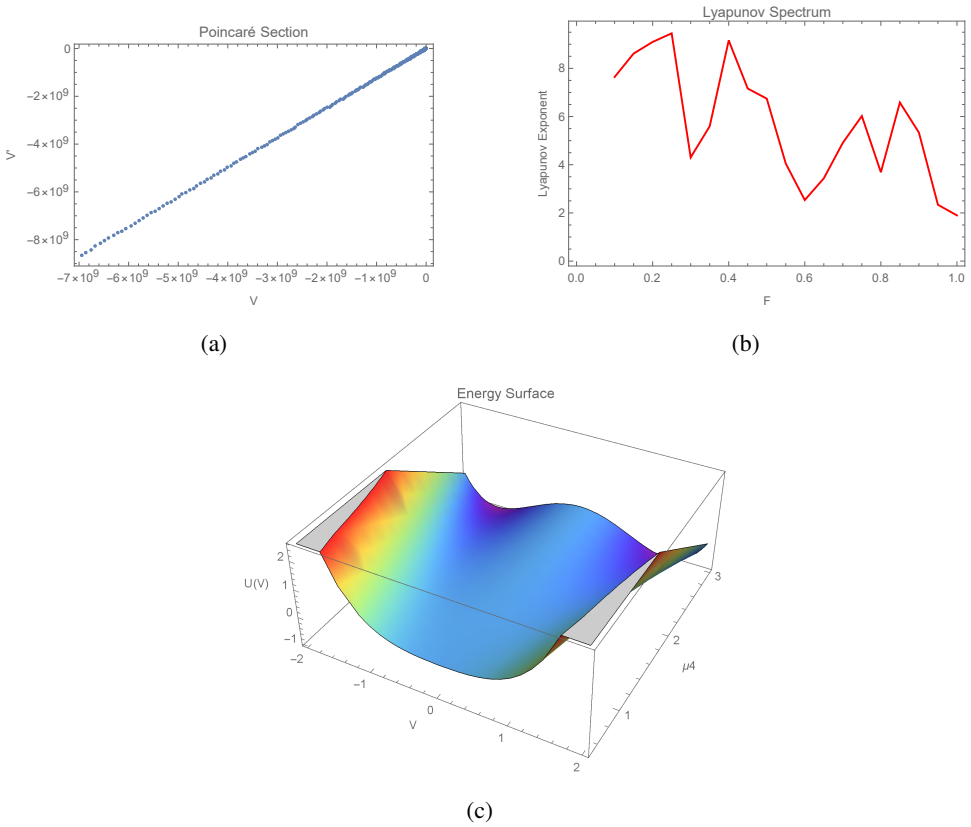
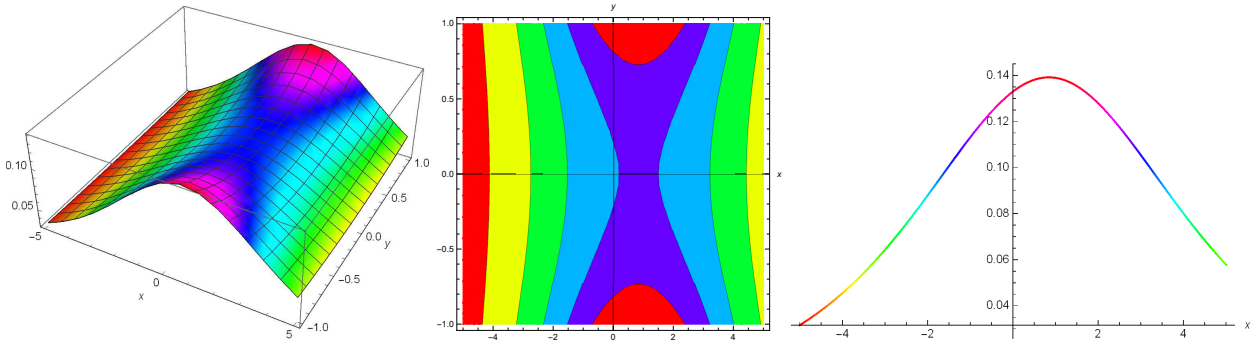


Figure 12. (a) The Poincaré section of the system as found by stroboscopic sampling at $\xi_n = 2\pi n/\omega$. The unique points reveal the phase space structure of the system. A fractal-like distribution confirms chaotic dynamics, while a limited number of points represents periodic behavior. (b) Variations in the control parameter's largest Lyapunov exponent. Positive values of the exponent confirm the presence of chaotic dynamics, while negative values show stable periodic motion. The transition point indicates the onset of chaos in the system. (c) Energy surface (Hamiltonian landscape) of the dynamical system illustrating the variation of total energy $E(x, y)$ in the phase space. The topology of the energy landscape clearly shows a transition from a single-well structure to a double-well potential as the control parameter μ_4 crosses the critical value μ_1, indicating bistability and phase space restructuring associated with bifurcation behavior.

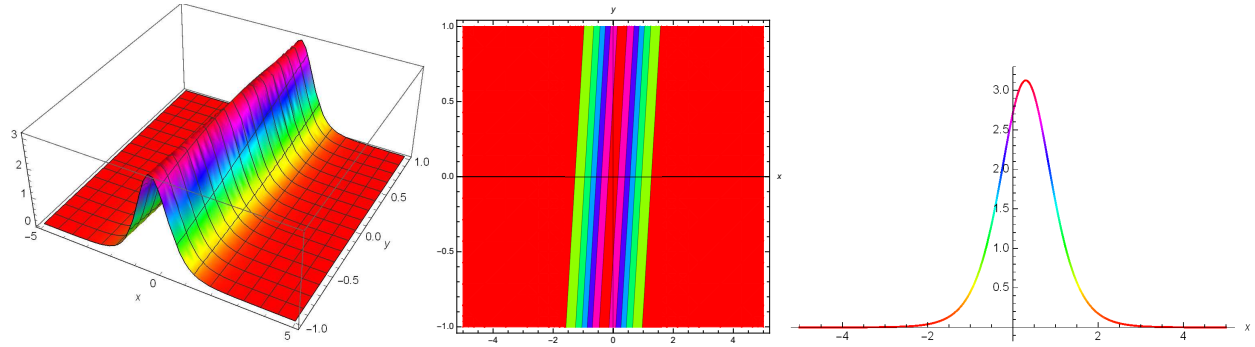
10. Discussion and results

In this section, the graphical description of the governing model (1.1) will be presented. A range of bright, singular bell-shaped, periodic, and dark solitons will be depicted for selected parameter values. Figure 13 depicts $|\Omega_2(x, y, t)|$ and shows the bright soliton for $\alpha = 0.1$, $\beta = 0.2$, $\gamma = 0.3$, $\alpha_0 = -0.6$, $\alpha_1 = 0.25$, $\alpha_3 = 0.5$, $\xi_0 = 0.2$, $\xi_2 = 0.4$, and $\xi_1 = 0.5$. Moreover, Figures 14 and 15 display the bright solitons. Figure 16 depicts $|\Omega_5(x, y, t)|$ and shows the singular bell-type soliton for $\alpha = 0.5$, $\beta = 0.6$, $\gamma = -0.7$, $\alpha_0 = 0.25$, $\alpha_1 = 1.2$, $\alpha_2 = -1.1$, $\beta_0 = 0.1$, $\beta_1 = 1.1$, $\beta_2 = -1.2$, $\beta_3 = 0.5$, and $\xi_1 = 0.25$. Similarly, Figures 17 and 18 display the singular bell-type solitons.



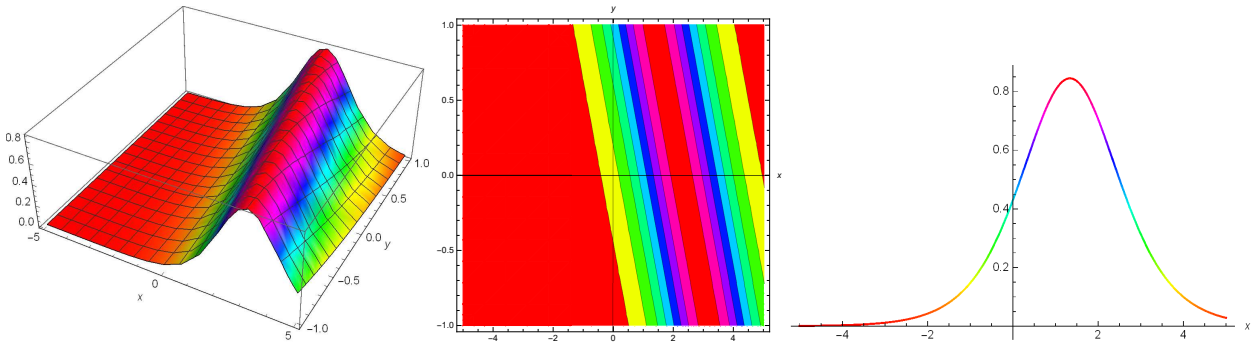
(a) (b) (c)

Figure 13. Portraits of the solution $|\Omega_2(x, y, t)|$ considering $\alpha_0 = -0.6$, $\alpha_1 = 0.25$, $\alpha_3 = 0.5$, $\gamma = 0.3$, $\alpha = 0.1$, $\xi_0 = 0.2$, $\xi_2 = 0.4$, $\xi_1 = 0.5$, and $\beta = 0.2$.



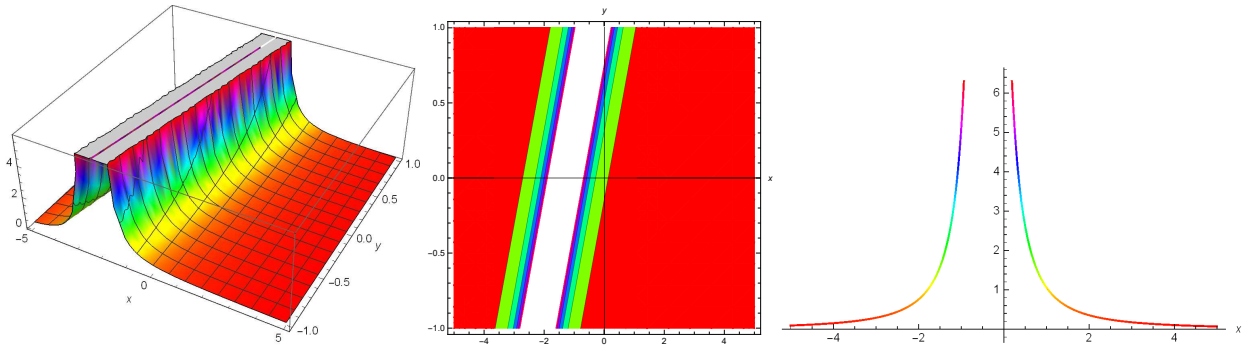
(a) (b) (c)

Figure 14. Portraits of the solution $|\Omega_3(x, y, t)|$ considering $\gamma_0 = 0.3$, $\gamma_1 = -2.5$, $\alpha = 0.5$, $\gamma_2 = 0.75$, $\xi_0 = 0.8$, $\gamma = 0.7$, $\xi_3 = 0.16$, and $\beta = 0.6$.



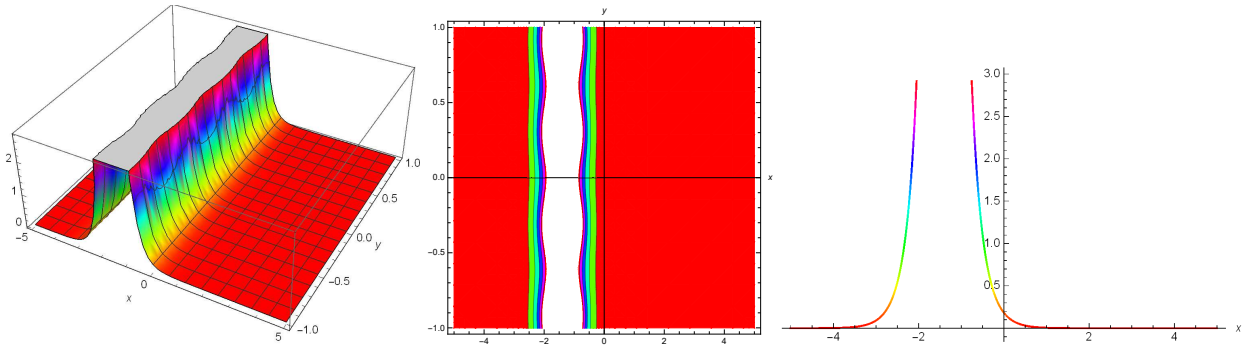
(a) (b) (c)

Figure 15. Portraits of the solution $|\Omega_7(x, y, t)|$ considering $\beta = 0.3$, $\gamma_0 = 0.5$, $\gamma_1 = 0.65$, $\alpha = 0.5$, $\gamma_2 = 0.6$, and $\gamma = 0.4$.



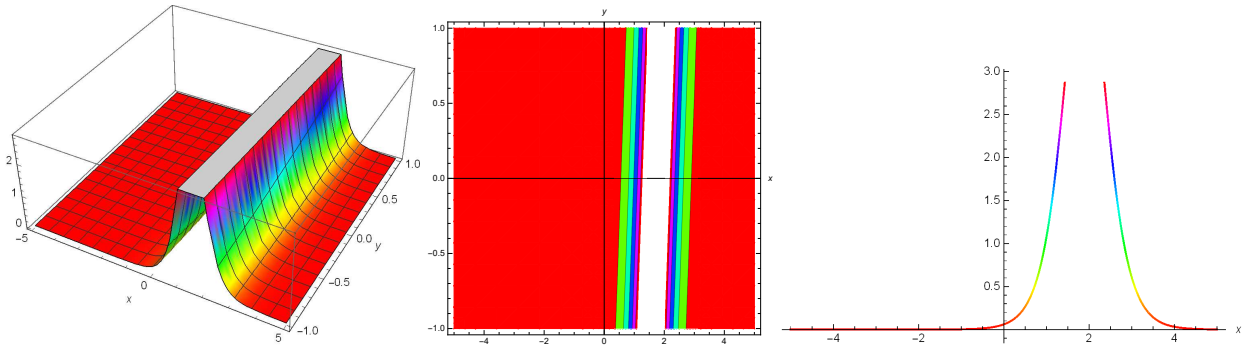
(a) (b) (c)

Figure 16. Portraits of the solution $|\Omega_5(x, y, t)|$ considering $\alpha_0 = 0.25$, $\alpha_1 = 1.2$, $\alpha_2 = -1.1$, $\beta_0 = 0.1$, $\alpha = 0.5$, $\beta_1 = 1.1$, $\beta_2 = -1.2$, $\beta = 0.6$, $\beta_3 = 0.5$, $\xi_1 = 0.25$, and $\gamma = -0.7$.



(a) (b) (c)

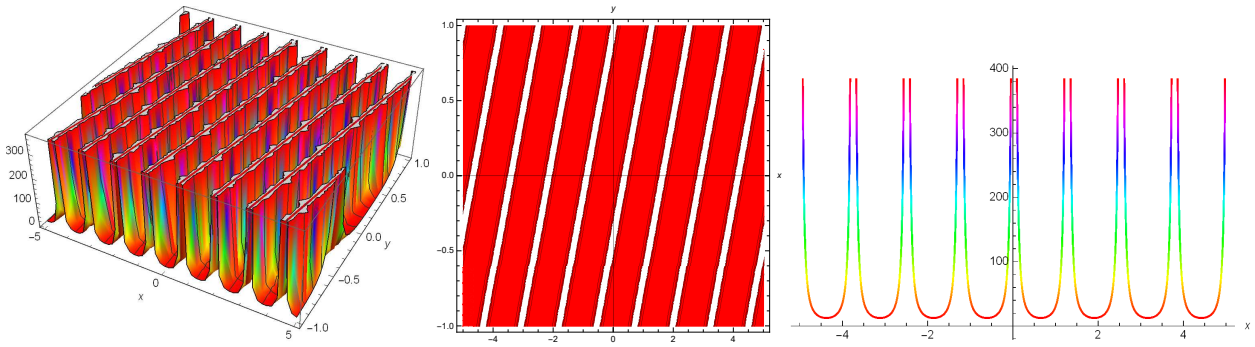
Figure 17. Portraits of the solution $|\Omega_{10}(x, y, t)|$ considering $\beta = 0.3$, $\gamma_0 = 1.55$, $\gamma_1 = 1.75$, $\alpha = 0.5$, $\gamma_3 = 0.9$, and $\gamma = 0.4$.



(a) (b) (c)

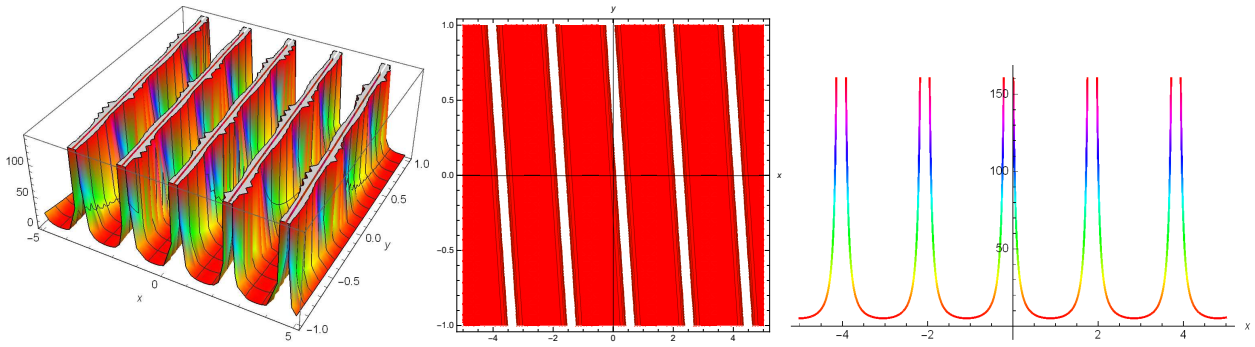
Figure 18. Portraits of the solution $|\Omega_{16}(x, y, t)|$ considering $\beta_0 = 0.55$, $\beta_1 = -1.5$, $\beta_2 = 0.255$, $\alpha = 2.1$, $\gamma_0 = 0.25$, $\xi_2 = 2.5$, $\beta = 0.2$, $\xi_3 = 0.45$, and $\gamma = 0.5$.

Figure 19 and 20 depict $|\Omega_{11}(x,y,t)|$ and $|\Omega_{13}(x,y,t)|$, and show the periodic waves for $\beta = 0.35$, $\gamma_0 = 0.2$, $\gamma_1 = 2.5$, $\alpha = 0.25$, $\gamma_2 = -2.3$, $\gamma = 0.45$ and $\beta = 0.2$, $\gamma_0 = 0.1$, $\gamma_1 = 1.6$, $\alpha = 0.1$, $\gamma_3 = 1.1$, $\gamma = 0.3$, respectively. Figure 21 depicts $|\Omega_{18}(x,y,t)|$ and shows the singular bell-type soliton for $a = -0.2$, $\kappa = -1.5$, $\omega = -1.6$, $\alpha = 0.25$, $\chi_1 = 1$, $\beta = -0.15$, $\chi_2 = 1.2$, $\gamma = 0.3$, and $b = -0.1$. Moreover, Figure 22 depicts $|\Omega_{21}(x,y,t)|$ and shows the dark soliton for $\kappa = -0.5$, $\omega = -0.6$, $\chi_1 = 1.2$, $\chi_2 = 1.5$, $a = 1.2$, $b = 1.1$, $\alpha = 1.25$, $\beta = 1.5$, and $\gamma = 1.3$. Lastly, Figure 23 depicts $|\Omega_{23}(x,y,t)|$ and shows the periodic wave soliton for $\kappa = 1.1$, $\omega = 1.6$, $\chi_1 = 1.5$, $\chi_2 = 1.2$, $a = 1.2$, $b = 1.1$, $\alpha = 1.25$, $\beta = 1.15$, and $\gamma = 1.3$.



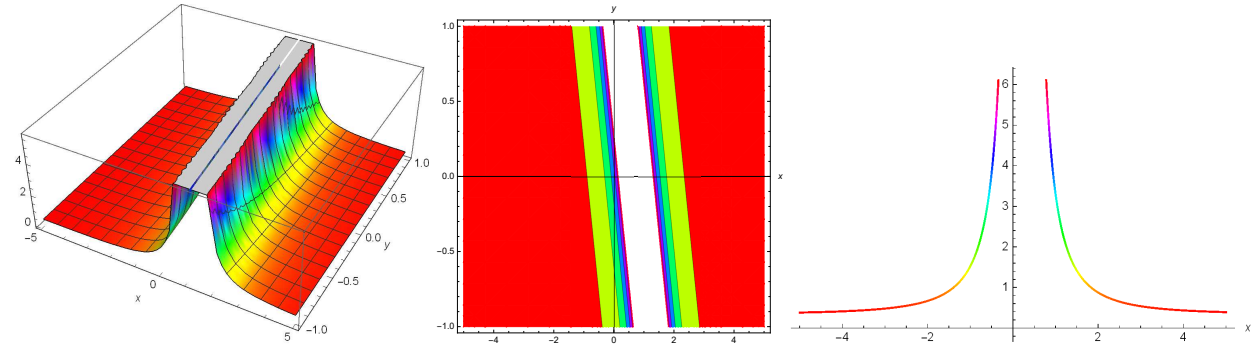
(a) (b) (c)

Figure 19. Portraits of the solution $|\Omega_{11}(x,y,t)|$ considering $\beta = 0.35$, $\gamma_0 = 0.2$, $\gamma_1 = 2.5$, $\alpha = 0.25$, $\gamma_2 = -2.3$, and $\gamma = 0.45$.



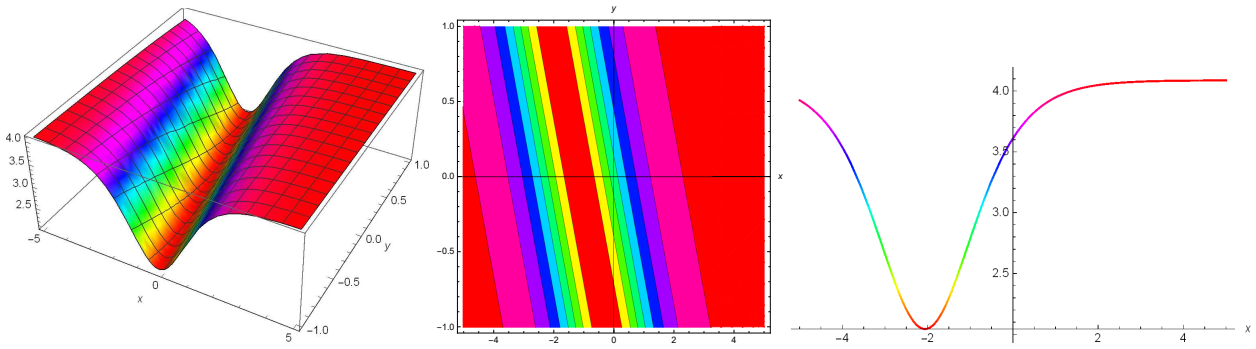
(a) (b) (c)

Figure 20. Portraits of the solution $|\Omega_{13}(x,y,t)|$ considering $\beta = 0.2$, $\gamma_0 = 0.1$, $\gamma_1 = 1.6$, $\alpha = 0.1$, $\gamma_3 = 1.1$, and $\gamma = 0.3$.



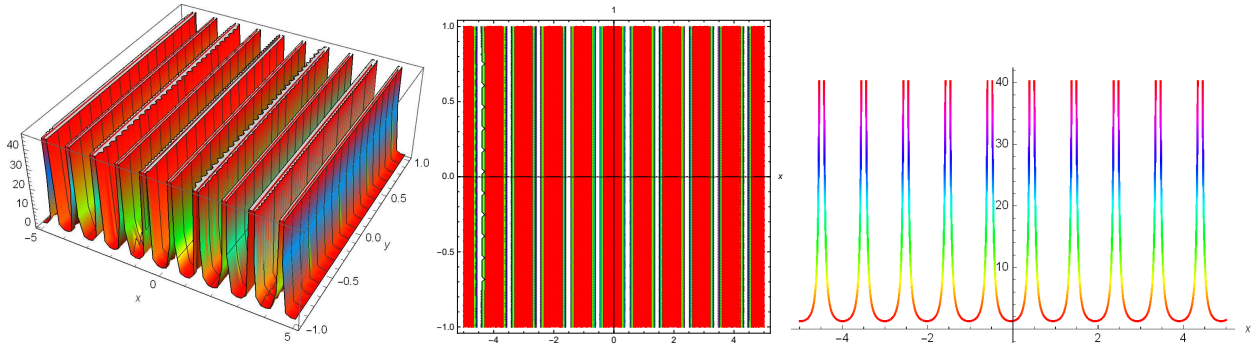
(a) (b) (c)

Figure 21. Portraits of the solution $|\Omega_{18}(x, y, t)|$ considering $a = -0.2$, $\kappa = -1.5$, $\omega = -1.6$, $\alpha = 0.25$, $\chi_1 = 1$, $\beta = -0.15$, $\chi_2 = 1.2$, $\gamma = 0.3$, and $b = -0.1$.



(a) (b) (c)

Figure 22. Portraits of the solution $|\Omega_{21}(x, y, t)|$ considering $a = 1.2$, $\kappa = -0.5$, $\alpha = 1.25$, $\omega = -0.6$, $\beta = 1.5$, $\chi_1 = 1.2$, $b = 1.1$, $\chi_2 = 1.5$, and $\gamma = 1.3$.



(a) (b) (c)

Figure 23. Portraits of the solution $|\Omega_{23}(x, y, t)|$ considering $\kappa = 1.1$, $\omega = 1.6$, $\chi_1 = 1.5$, $\chi_2 = 1.2$, $a = 1.2$, $b = 1.1$, $\alpha = 1.25$, $\beta = 1.15$, and $\gamma = 1.3$.

11. Conclusions

We studied diffusive long waves and bidirectional compact structures in a dissipative stratified medium using the (2+1)-dimensional KP-BBM equation. Hirota's bilinear method produced lump solutions, periodic waves interacting with double strip solitons, and lump interactions with single and double strip solitons. Additional exact traveling-wave solutions emerged using the (G'/G^2)-expansion method, and numerical ones were obtained using the Adomian decomposition methodology. Phase-plane analysis and traveling-wave reduction revealed bifurcations and changes from periodic to chaotic motion, which were verified by Poincaré sections and Lyapunov exponents. Sensitivity and stability studies verified that the wave structures can withstand minor disturbances and revealed which characteristics are most important. The resulting soliton family includes bright, dark, rational, periodic, and elliptic-function types. These findings reveal that the KP-BBM equation supports a broader range of nonlinear wave phenomena than previously recognized. Future work could extend the analysis to variable-coefficient models or seek experimental confirmation in stratified fluid experiments.

Author contributions

Kalim U. Tariq: Conceptualization, Supervision, Project administration, Methodology, Resources; Mohammed Ahmed Alomair: Software, Validation, Visualization, Funding acquisition, Review and editing; R. Nadir Tufail: Formal analysis, Investigation, Writing–original draft. All authors have read and approved the final version of the manuscript for publication.

Use of Generative-AI tools declaration

The authors declare they have not used Artificial Intelligence (AI) tools in the creation of this article.

Acknowledgements

This work was supported by the Deanship of Scientific Research, Vice Presidency for Graduate Studies and Scientific Research, King Faisal University, Saudi Arabia [Grant No. KFU265050].

Conflict of interest

The authors declare that they have no conflicts of interest.

References

1. F. Badshah, Ammara, S. Asghar, Ziauddin, S. H. Dong, Investigation of diffraction grating in three-level gain medium, *Opt. Laser Technol.*, **177** (2024), 111104. https://doi.org/10.1016/j.optlastec.2024.111104
2. K. U. Tariq, M. Inc, A. Pashrashide, M. Zubair, L. Akinyemi, On the structure of unsteady Korteweg-de Vries model arising in shallow water, *J. Ocean Eng. Sci.*, 2022, In press. https://doi.org/10.1016/j.joes.2022.01.011

3. F. Badshah, K. U. Tariq, A. Bekir, R. N. Tufail, H. Ilyas, Lump, periodic, travelling, semi-analytical solutions and stability analysis for the Ito integro-differential equation arising in shallow water waves, *Chaos Solitons Fract.*, **182** (2024), 114783. https://doi.org/10.1016/j.chaos.2024.114783
4. K. U. Tariq, A. Bekir, S. Nisar, The dynamical structures of the Sharma-Tasso-Olver model in doubly dispersive medium, *Chaos Solitons Fract.*, **177** (2023), 114290. https://doi.org/10.1016/j.chaos.2023.114290
5. A. R. Seadawy, A. Ali, A. Bekir, A. C. Cevikel, Ö. Guner, Novel exact wave solutions of the (4+1)-dimensional Boiti-Leon-Manna-Pempinelli model via application of three mathematical methods, *Opt. Quantum Electron.*, **56** (2024), 1143. https://doi.org/10.1007/s11082-024-06997-1
6. S. T. R. Rizvi, S. Ahmed, Resonant collisions among X-type, multi-lump, generalized breathers, N-solitons and rogue waves in plasma, *Optik*, **292** (2023), 171390. https://doi.org/10.1016/j.ijleo.2023.171390
7. K. U. Tariq, A. R. Seadawy, S. T. R. Rizvi, R. Javed, Some optical soliton solutions to the generalized (1+1)-dimensional perturbed nonlinear Schrödinger equation using two analytical approaches, *Int. J. Mod. Phys. B*, **36** (2022), 2250177. https://doi.org/10.1142/S0217979222501776
8. M. Inc, New solitary wave solutions with compact support and Jacobi elliptic function solutions for the nonlinearly dispersive Boussinesq equations, *Chaos Solitons Fract.*, **37** (2008), 792–798. https://doi.org/10.1016/j.chaos.2006.09.064
9. F. Badshah, K. U. Tariq, A. Bekir, On the solitonic wave structures for the perturbed nonlinear Schrödinger equation arising in optical fibers, *Opt. Quantum Electron.*, **56** (2024), 127. https://doi.org/10.1007/s11082-023-05625-8
10. D. Kumar, K. Hosseini, F. Samadani, The sine-Gordon expansion method to look for the traveling wave solutions of the Tzitzéica type equations in nonlinear optics, *Optik*, **149** (2017), 439–446. https://doi.org/10.1016/j.ijleo.2017.09.066
11. T. Islam, A. Akbar, H. Rezazadeh, A. Bekir, New-fashioned solitons of coupled nonlinear Maccari systems describing the motion of solitary waves in fluid flow, *J. Ocean Eng. Sci.*, **9** (2024), 353–363. https://doi.org/10.1016/j.joes.2022.03.003
12. S. Carillo, M. L. Schiavo, C. Schiebold, Bäcklund transformations and non-abelian nonlinear evolution equations: a novel Bäcklund chart, *SIGMA*, **12** (2016), 087. https://doi.org/10.3842/SIGMA.2016.087
13. C. Q. Dai, Y. Y. Wang, Notes on the equivalence of different variable separation approaches for nonlinear evolution equations, *Commun. Nonlinear Sci. Numer. Simul.*, **19** (2014), 19–28. https://doi.org/10.1016/j.cnsns.2013.05.027
14. X. G. Geng, G. L. He, Some new integrable nonlinear evolution equations and Darboux transformation, *J. Math. Phys.*, **51** (2010), 033514. https://doi.org/10.1063/1.3355192
15. E. Misirli, Y. Gurefe, Exp-function method for solving nonlinear evolution equations, *Math. Comput. Appl.*, **16** (2011), 258–266. https://doi.org/10.3390/mca16010258
16. K. U. Tariq, A. M. Wazwaz, R. N. Tufail, Lump, periodic and travelling wave solutions to the (2+1)-dimensional pKP-BKP model, *Eur. Phys. J. Plus*, **137** (2022), 1–22. https://doi.org/10.1140/epjp/s13360-022-03301-6

17. Z. B. Yu, C. H. Zhu, J. S. Zhao, L. Zou, Inverse scattering transform of the general three-component nonlinear Schrödinger equation and its multisoliton solutions, *Appl. Math. Lett.*, **128** (2022), 107874. https://doi.org/10.1016/j.aml.2021.107874
18. S. W. Yao, K. U. Tariq, M. Inc, R. N. Tufail, Modulation instability analysis and soliton solutions of the modified BBM model arising in dispersive medium, *Results Phys.*, **46** (2023), 106274. https://doi.org/10.1016/j.rinp.2023.106274
19. M. Mirzazadeh, A. Akbulut, F. Tascan, L. Akinyemi, A novel integration approach to study the perturbed Biswas-Milovic equation with Kudryashov's law of refractive index, *Optik*, **252** (2022), 168529. https://doi.org/10.1016/j.ijleo.2021.168529
20. M. A. Abdelkawy, A. H. Bhrawy, E. Zerrad, A. Biswas, Application of tanh method to complex coupled nonlinear evolution equations, *Acta Phys. Polon. A*, **129** (2016), 278–283. https://doi.org/10.12693/APhysPolA.129.278
21. R. C. López, G. H. Sun, O. Camacho-Nieto, C. Yáñez-Márquez, S. H. Dong, Analytical traveling-wave solutions to a generalized Gross-Pitaevskii equation with some new time and space varying nonlinearity coefficients and external fields, *Phys. Lett. A*, **381** (2017), 2978–2985. https://doi.org/10.1016/j.physleta.2017.07.012
22. X. L. Mai, W. Li, S. H. Dong, Exact solutions to the nonlinear Schrödinger equation with time-dependent coefficients, *Adv. High Energy Phys.*, **2021** (2021), 6694980. https://doi.org/10.1155/2021/6694980
23. W. Li, C. F. Jiang, J. W. Huo, Y. S. Guo, Y. Shen, S. H. Dong, Gaussian solitary-wave solutions of a generalized logarithmic nonlinear Schrödinger equation with external potentials, *Phys. Lett. A*, **592** (2026), 131984. https://doi.org/10.1016/j.physleta.2026.131984
24. W. X. Ma, Lump solutions to the Kadomtsev-Petviashvili equation, *Phys. Lett. A*, **379** (2015), 1975–1978. https://doi.org/10.1016/j.physleta.2015.06.061
25. A. M. Wazwaz, Exact solutions of compact and noncompact structures for the KP-BBM equation, *Appl. Math. Comput.*, **169** (2005), 700–712. https://doi.org/10.1016/j.amc.2004.09.061
26. A. M. Wazwaz, Two new integrable Kadomtsev-Petviashvili equations with time-dependent coefficients: multiple real and complex soliton solutions, *Waves Random Complex Media*, **30** (2020), 776–786. https://doi.org/10.1080/17455030.2018.1559962
27. A. R. Seadawy, Travelling-wave solutions of a weakly nonlinear two-dimensional higher-order Kadomtsev-Petviashvili dynamical equation for dispersive shallow-water waves, *Eur. Phys. J. Plus*, **132** (2017), 29. https://doi.org/10.1140/epjp/i2017-11313-4
28. M. A. Salam, M. A. Akbar, M. Z. Ali, M. Inc, The higher-order nonlinearity and parametric effects on dust-ion-acoustic shock waves, *Phys. Scr.*, **97** (2022), 125605. https://doi.org/10.1088/1402-4896/ac9dc8
29. H. Rezazadeh, M. Inc, D. Baleanu, New solitary wave solutions for variants of (3+1)-dimensional Wazwaz-Benjamin-Bona-Mahony equations, *Front. Phys.*, **8** (2020), 332. https://doi.org/10.3389/fphy.2020.00332
30. A. M. Wazwaz, H. Triki, Soliton solutions for a generalized KdV and BBM equations with time-dependent coefficients, *Commun. Nonlinear Sci. Numer. Simul.*, **16** (2011), 1122–1126. https://doi.org/10.1016/j.cnsns.2010.06.024

31. A. M. Wazwaz, The extended tanh method for new compact and noncompact solutions for the KP-BBM and the ZK-BBM equations, *Chaos Solitons Fract.*, **38** (2008), 1505–1516. https://doi.org/10.1016/j.chaos.2007.01.135

32. J. C. Saut, N. Tzvetkov, Global well-posedness for the KP-BBM equations, *Appl. Math. Res. eXpress*, **2004** (2004), 1–16. https://doi.org/10.1155/S1687120004010718

33. M. N. Alam, M. A. Akbar, Exact traveling wave solutions of the KP-BBM equation by using the new approach of generalized (G'/G)-expansion method, *SpringerPlus*, **2** (2013), 617. https://doi.org/10.1186/2193-1801-2-617

34. S. Q. Tang, X. L. Huang, W. T. Huang, Bifurcations of travelling wave solutions for the generalized KP-BBM equation, *Appl. Math. Comput.*, **216** (2010), 2881–2890. https://doi.org/10.1016/j.amc.2010.03.139

35. J. Q. Lü, S. Bilige, X. Q. Gao, Y. X. Bai, R. F. Zhang, Abundant lump solutions and interaction phenomena to the Kadomtsev-Petviashvili-Benjamin-Bona-Mahony equation, *J. Appl. Math. Phys.*, **6** (2018), 1733–1747. https://doi.org/10.4236/jamp.2018.68148

36. J. Tan, Z. H. Deng, T. L. Wu, B. Tang, Propagation and interaction of magnetic solitons in a ferromagnetic thin film with the interfacial Dzyaloshinskii-Moriya interaction, *J. Magn. Magn. Mater.*, **475** (2019), 445–452. https://doi.org/10.1016/j.jmmm.2018.11.048

37. Z. H. Deng, T. L. Wu, B. Tang, X. Y. Wang, H. P. Zhao, K. Deng, Breathers and rogue waves in a ferromagnetic thin film with the Dzyaloshinskii-Moriya interaction, *Eur. Phys. J. Plus*, **133** (2018), 450. https://doi.org/10.1140/epjp/i2018-12311-8

38. Z. H. Deng, X. Chang, J. N. Tan, B. Tang, K. Deng, Characteristics of the lumps and stripe solitons with interaction phenomena in the (2+1)-dimensional Caudrey-Dodd-Gibbon-Kotera-Sawada equation, *Int. J. Theor. Phys.*, **58** (2019), 92–102. https://doi.org/10.1007/s10773-018-3912-2

39. S. F. Tian, Lie symmetry analysis, conservation laws and solitary wave solutions to a fourth-order nonlinear generalized Boussinesq water wave equation, *Appl. Math. Lett.*, **100** (2020), 106056. https://doi.org/10.1016/j.aml.2019.106056

40. H. Wang, S. F. Tian, T. T. Zhang, Y. Chen, Y. Fang, General lump solutions, lumpoff solutions, and rogue wave solutions with predictability for the (2+1)-dimensional Korteweg-de Vries equation, *Comput. Appl. Math.*, **38** (2019), 164. https://doi.org/10.1007/s40314-019-0938-x

41. W. Q. Peng, S. F. Tian, X. B. Wang, T. T. Zhang, Y. Fang, Riemann-Hilbert method and multi-soliton solutions for three-component coupled nonlinear Schrödinger equations, *J. Geom. Phys.*, **146** (2019), 103508. https://doi.org/10.1016/j.geomphys.2019.103508

42. W. Q. Peng, S. F. Tian, X. B. Wang, T. T. Zhang, Characteristics of rogue waves on a periodic background for the Hirota equation, *Wave Motion*, **93** (2020), 102454. https://doi.org/10.1016/j.wavemoti.2019.102454

43. D. Guo, S. F. Tian, X. B. Wang, T. T. Zhang, Dynamics of lump solutions, rogue wave solutions and traveling wave solutions for a (3+1)-dimensional VC-BKP equation, *East Asian J. Appl. Math.*, **9** (2019), 780–796. https://doi.org/10.4208/eajam.310319.040619

44. W. Q. Peng, S. F. Tian, T. T. Zhang, Dynamics of the soliton waves, breather waves, and rogue waves to the cylindrical Kadomtsev-Petviashvili equation in pair-ion-electron plasma, *Phys. Fluids*, **31** (2019), 102107. https://doi.org/10.1063/1.5116231

45. W. Q. Peng, S. F. Tian, T. T. Zhang, Dynamics of breather waves and higher-order rogue waves in a coupled nonlinear Schrödinger equation, *Europhys. Lett.*, **123** (2018), 50005. https://doi.org/10.1209/0295-5075/123/50005

46. R. Hirota, Exact solution of the Korteweg-de Vries equation for multiple collisions of solitons, *Phys. Rev. Lett.*, **27** (1971), 1192. https://doi.org/10.1103/PhysRevLett.27.1192

47. W. X. Ma, Y. Zhou, Lump solutions to nonlinear partial differential equations via Hirota bilinear forms, *J. Differ. Equ.*, **264** (2018), 2633–2659. https://doi.org/10.1016/j.jde.2017.10.033

48. R. Hirota, *The direct method in soliton theory*, Cambridge University Press, 2004. https://doi.org/10.1017/CBO9780511543043

49. A. Wolf, J. B. Swift, H. L. Swinney, J. A. Vastano, Determining Lyapunov exponents from a time series, *Phys. D*, **16** (1985), 285–317. https://doi.org/10.1016/0167-2789(85)90011-9



AIMS Press

© 2026 the Author(s), licensee AIMS Press. This is an open access article distributed under the terms of the Creative Commons Attribution License (https://creativecommons.org/licenses/by/4.0)